

**An-Najah- National University**  
**Faculty of Graduate Studies**

**FP-LAPW STUDY OF PHASE  
CHANGES IN AN (A=Al, In, and B)  
UNDER HIGH PRESSURE**

**By**  
**Haneen Yousef Saeed Shalash**

**Supervisors**  
**Dr. Mohammed S. Abu-Jafar**  
**Dr. Abdel-Rahman M.Abu-Labdeh**

**This Thesis is Submitted in Partial Fulfillment of the Requirements for  
the Degree of Master of Science in Physics, Faculty of Graduate  
studies, An-Najah National University, Nablus, Palestine.**

**2009**

**FP-LAPW STUDY OF PHASE CHANGES  
IN AN (A=Al,In, and B) UNDER HIGH PRESSURE**

**By  
Haneen Yousef Saeed Shalash**

**This Thesis was defended successfully on 9/7/2009 and approved by:**

**Defense Committee Members**

**Signature**

**1. Dr. Mohammed Abu-Jafar(Supervisor)**

*Moh'd S. Saeed*  
-----

**2. Dr. Abdel-Rahman Abu-Labdeh(Co-Supervisor)**

-----  
*RL*

**3. Dr. Rushdi Kitaneh (External Examiner)**

-----  
*RK*

**4. Dr. Musa El-Hasan(Internal Examiner)**

-----  
*MEH*

## **Dedicated to**

I do dedicate this work to the dearest people to my heart:  
to my mother, father, husband, and to my son Harith.

## **Acknowledgment**

**I do thank Allah for allowing me to finish this thesis successfully. My deepest gratitude and appreciation to my dear supervisors, Dr. Mohammed Abu Jafar and Dr. Abdel-Rahman Abu-Labdeh for helping and guiding me with their deep knowledge in my field of study and to complete the thesis.**

**Thanks to the Defense Committee Members and also to all my family members: My father, my husband's family, brothers and sisters, especially to my mother, my brother mohaned and husband for their encouragement, support, patient and precious help.**

## الإقرار

أنا الموقع أدناه مقدم الرسالة التي تحمل العنوان:

## FP-LAPW STUDY OF PHASE CHANGES IN AN (A=Al, In, and B) UNDER HIGH PRESSURE

دراسة تغيرات الحالة لكل من المركبات نيتريد الألمنيوم  
ونيتريد البورون ونيتريد الإنديوم تحت ضغط عال باستخدام  
طريقة FP-LAPW

أقر بأن ما اشتملت عليه هذه الرسالة إنما هي نتاج جهدي الخاص، باستثناء ما تمت الإشارة إليه حيثما ورد، وأن هذه الرسالة ككل، أو أي جزء منها لم يقدم من قبل لنيل أية درجة علمية أو بحث علمي أو بحثي لدى أية مؤسسة تعليمية أو بحثية أخرى.

### Declaration

The work provided in this thesis, unless otherwise referenced, is the researcher's own work, and has not been submitted elsewhere for any other degree or qualification.

Student's name:

اسم الطالب:

Signature:

التوقيع:

Date:

التاريخ:

## Table of Contents

No.	Content	Page
	Dedication	iii
	Acknowledgment	iv
	Declaration	v
	Table of Contents	vi
	List of tables	vii
	List of figures	viii
	Abstract	x
	<b>Chapter 1 Introduction</b>	<b>1</b>
	<b>Chapter 2 Methodology</b>	<b>9</b>
2.1	Density functional theory	9
2.2	Kohn Sham Equations	16
2.3	Local Density Approximation	19
2.4	Generalized Gradient Approximation	25
2.5	The FP-LAPW method	27
	<b>Chapter 3 Computational Details</b>	<b>33</b>
3.1	Wurtzite Structure	33
3.2	Rocksalt Structure	34
3.3	Zincblende Structure	35
3.4	The Computational Details	36
	<b>Chapter 4 Results And Discussion</b>	<b>41</b>
4.1	AlN Compound	41
4.1.1	Structural Properties	41
4.1.1.a	Wurtzite-AlN structure	42
4.1.1.b	Zincblende-AlN structure	44
4.1.1.c	Rocksalt- AlN structure	46
4.1.2	Band Structure	47
4.1.3	Structural phase transition	52
4.2	BN Compound	55
4.2.1	Structural Properties	55
4.2.2	Band Structure	58
4.2.3	Structural phase transition	60
4.3	InN Compound	61
4.3.1	Structural Properties	61
4.3.2	Band Structure	66
4.3.3	Structural phase transition	<b>70</b>
	<b>Chapter 5 Conclusion</b>	<b>71</b>
	<b>References</b>	<b>73</b>
	المخلص	ب

### List of Tables

No.	Table	Page
<b>Table (3.1)</b>	L- expansion of the non spherical potential and energy using GGA and LDA approximations for RS-AlN	37
<b>Table (4.1)</b>	The calculated lattice parameters for AlN, BN, and InN using LDA Method	42
<b>Table (4.2)</b>	The calculated lattice parameters for AlN, BN, InN using GGA Method	42
<b>Table (4.3)</b>	The structural parameters for wurtzite-AlN structure using LDA and GGA methods	42
<b>Table (4.4)</b>	The structural parameters for zincblende-AlN structure using LDA and GGA Methods	44
<b>Table (4.5)</b>	The structural parameters for rocksalt-AlN structure using LDA and GGA methods	46
<b>Table (4.6)</b>	The energy band structures for AlN compound in WZ, RS, and ZB structures	48
<b>Table (4.7)</b>	Transition pressure of AlN structure using LDA and GGA methods	53
<b>Table (4.8)</b>	The structural parameters for zincblende-BN structure using LDA and GGA methods	55
<b>Table (4.9)</b>	The structural parameters for rocksalt-BN structure using LDA and GGA methods	57
<b>Table (4.10)</b>	The energy band gap for BN compound	58
<b>Table (4.11)</b>	Transition pressure of BN structure using GGA method	60
<b>Table (4.12)</b>	The structural parameters for Wurtzite-InN structure using LDA and GGA methods	62
<b>Table (4.13)</b>	The structural parameters for Rocksalt-InN structure using LDA and GGA methods	63
<b>Table (4.14)</b>	The structural parameters for ZB-InN structure using LDA and GGA methods	65
<b>Table (4.15)</b>	The energy band structures for InN compound	66
<b>Table (4.16)</b>	Transition pressure of InN structure using GGA method	70

## List of Figures

No.	Figure	Page
<b>Figure (2.1)</b>	Flow chart of solving the self-consistent Kohn-Sham equation	18
<b>Figure (2.2)</b>	Summary of the electron-electron interactions (excluding coulomb effects) in (a) the Hartree approximation, (b) the Hartree-Fock approximation, (c) the local density approximation and (d) the local spin density approximation which allows for different interactions for like-unlike spins	24
<b>Figure (2.3)</b>	Partitioning of the unit cell into atomic spheres (I) and an interstitial region (II)	29
<b>Figure (3.1)</b>	The primitive unit cell of AlN in Wurtzite structure	33
<b>Figure (3.2)</b>	The conventional unit cell of AlN in the Wurtzite structure	34
<b>Figure (3.3)</b>	The primitive unit cell of AlN in Rocksalt structure	34
<b>Figure (3.4)</b>	The conventional unit cell of AlN in the Rocksalt structure	35
<b>Figure (3.5)</b>	The primitive unit cell of AlN in Zincblende structure	35
<b>Figure (3.6)</b>	The conventional unit cell of AlN in the Zincblende structure	36
<b>Figure (3.7)</b>	The convergent test using GGA approximation for RS-AlN	38
<b>Figure (3.8)</b>	The convergent test using LDA approximation for RS-AlN	38
<b>Figure (4.1)</b>	Energy versus volume for WZ-AlN using GGA method	43
<b>Figure (4.2)</b>	Energy versus volume for WZ-AlN using LDA method	44
<b>Figure (4.3)</b>	Energy versus volume for ZB-AlN using GGA method	45
<b>Figure (4.4)</b>	Energy versus volume for ZB-AlN using LDA method	45
<b>Figure (4.5)</b>	Energy versus volume for RS-AlN using LDA method	46
<b>Figure (4.6)</b>	Energy versus volume for RS-AlN using GGA method	47
<b>Figure (4.7)</b>	The energy band structures for wurzite AlN using GGA and LDA methods	50
<b>Figure (4.8)</b>	The energy band structures for rocksalt AlN using GGA and LDA methods	51
<b>Figure (4.9)</b>	The energy band structures for zincblende AlN using GGA and LDA	52
<b>Figure (4.10)</b>	The transition pressure of AlN using GGA method	54

<b>No.</b>	<b>Figure</b>	<b>Page</b>
<b>Figure (4.11)</b>	The transition pressure of AlN using LDA method	54
<b>Figure (4.12)</b>	Energy versus volume for ZB-BN using GGA method	56
<b>Figure (4.13)</b>	Energy versus volume for ZB-BN using LDA method	56
<b>Figure (4.14)</b>	Energy versus volume for RS-BN using LDA method	57
<b>Figure (4.15)</b>	Energy versus volume for RS-BN using GGA method	58
<b>Figure (4.16)</b>	The energy band structures for zincblende BN using GGA and LDA methods	59
<b>Figure (4.17)</b>	The energy band gap for rocksalt BN using GGA and LDA methods	60
<b>Figure (4.18)</b>	The transition pressure of BN using GGA method	61
<b>Figure (4.19)</b>	Energy versus volume for WZ-InN using LDA method	62
<b>Figure (4.20)</b>	Energy versus volume for WZ-InN using GGA method	63
<b>Figure (4.21)</b>	Energy versus volume for RS-InN using GGA method	64
<b>Figure (4.22)</b>	Energy versus volume for RS -InN using LDA method	64
<b>Figure (4.23)</b>	Energy versus volume for ZB-InN using LDA method	65
<b>Figure (4.24)</b>	Energy versus volume for ZB-InN using GGA method	66
<b>Figure (4.25)</b>	The energy band structures for wurzite InN using GGA and LDA methods	67
<b>Figure (4.26)</b>	The energy band structures for zincblende InN using GGA and LDA methods	68
<b>Figure (4.27)</b>	The energy band structures for rocksalt InN using GGA and LDA methods	69
<b>Figure (4.28)</b>	The transition pressure of InN using GGA method	70

**FP-LAPW STUDY OF PHASE CHANGES IN AN (A=Al, In, and B)  
UNDER HIGH PRESSURE**

**By**

**Haneen Yousef Saeed Shalash**

**Supervisors**

**Dr. Mohammed S. Abu-Jaafar**

**Dr. Abdel-Rahman M. Abu-Labdeh**

**Abstract**

In the last few years no other class of material of semiconductors has attracted so much scientific and commercial attention like the group III-nitrides (AlN, BN, and InN). The increasing interest is due to its extraordinary physical properties, which can be used in many new electronic and optoelectronic devices. The AlN is stable to very high temperatures in inert atmospheres. Another stable material in inert and reducing atmospheres is BN. It is a very good electrical insulator. It offers very high thermal conductivity and good thermal shock resistance. InN has attracted considerable attention due to the repeated observation of an effective band gap in the range around 0.7 eV by optical techniques, this smaller band gap value would extend the possible emission range of optoelectronic devices based on III-nitrides from the deep-UV down to the near-IR region.

Very prominent examples are the short wavelength Light emitting diodes (LED's) and laser diodes, which take advantage of the wide band gap of AlN. InN also has been expected to be a suitable material for electronic devices such as high mobility transistors due to its small effective mass.

The effect of pressure on the electronic properties of (AlN, BN, and InN) are investigated using both experimental and theoretical methods. In

this study, we carry out all-electron full potential linearized-augmented plane waves (FP-LAPW) (which is included in a computer code WIEN2K) approach within the density functional theory (DFT) in the local density approximation (LDA), and the generalized gradient approximation (GGA) for the exchange correlations functional, which used to calculate ground-state energies, the lattice parameters, the bulk modulus and its derivatives, transition pressure and the band structures. The equation of state of wurtzite (WZ), zincblende(ZB) and rocksalt(RS) structures for (AlN, BN, and InN) compounds have been calculated.

In this study, the most important results are:

1. The present calculations agree very well with available experimental data and other theoretical calculations.
2. AlN compound behaves as an insulator in (WZ, ZB, and RS) structures.
3. BN compound behaves as a semiconductor for RS and ZB in LDA calculation and an insulator for RS and ZB in GGA calculation.
4. InN compound behaves as a semimetal in (WZ, ZB, and RS) structures.
5. The energy band gap for (WZ, RS, and ZB ) structures of AlN are found to be (4.42, 4.032, 2.7) eV respectively, using LDA method, and (4.17, 4.34, 3.275) eV respectively, using GGA method.

6. The energy band gap for (ZB and RS) structures of BN are found to be (4.36, 2.193) eV respectively, using LDA method, and (4.43, 1.71) eV respectively, using GGA method.
7. The energy band gap for (WZ, RS, and ZB ) structures of InN are found to be ( -0.264, 0.0838, -0.3896) eV respectively, using LDA method, and (-0.3643, -0.277, -0.5136) eV respectively, using GGA method.
8. For AlN the transition pressure from wurtzite to rocksalt was found to be (10) GPa and from zincblende to rocksalt was found to be (4.64) GPa using GGA method, while the transition pressure from wurtzite to rocksalt was found to be 9.3 GPa and from zincblende to rocksalt was found to be 3 GPa using LDA method.
9. For InN the transition pressure from wurtzite to rocksalt was found to be 16.6 GPa and from zincblende to rocksalt was found to be 18.5 GPa using GGA method.
10. The transition pressure for BN compound from zincblende to rocksalt was found to be 500 GPa using GGA method.

## **Chapter 1**

### **Introduction**

Today, semiconductor materials constitute basic building blocks of emitters and receivers in cellular, satellite, and fiberglass communication. One important class of semiconductor material is the III-nitrides such as BN, AlN, and InN. These semiconductor materials have also received considerable attention for their device applications in blue and ultraviolet wavelengths [1, 2, 3]. Recently, the successful fabrication of the blue light III-nitrides semiconductor laser was first demonstrated by Nakamura [4]. The vast majority of research on III- nitrides has been focused on the wurtzite crystal phase, because the sapphire substrates tend to transfer their hexagonal symmetry to the nitride films grown on them [2]. However, interest in zincblende nitrides has been growing recently.

The dependence of photoluminescence on pressure is very useful in the understanding of electronic energy band structure and structural properties in semiconductors. The effect of pressure on the electronic properties of III–nitride compounds can be investigated experimentally in many ways[2]. The technical development of epitaxial growth at the end of the last century has provided the possibility for researchers to fabricate synthetic materials with expected compositions and structures. On the other hand, theoretical and technical developments in density-functional theory (DFT) and pseudopotential calculations in recent decades have provided researchers with powerful methods for predicting electronic and energetic properties as revealed by novel experimental techniques. This has

stimulated extensive computational studies on high-pressure behavior of various semiconductors [2].

The electronic properties of the zincblende and wurtzite group III-nitride compound semiconductors (AlN, GaN, and InN) were studied within the empirical pseudopotential approach [5]. Using ionic model potentials and the static dielectric screening function derived by Levine and Louie [6], the cationic and anionic model potential parameters were obtained from zincblende AlN, GaN, and InN experimental data. By using the concept of transferable model potentials, Levine and Louie also, calculated the band structure of group-III nitrides in zincblende and wurtzite phase using the same ionic model potential parameters[6]. Self-consistent linear muffin-tin-orbital band-structure calculations were used to investigate the optical and structural properties of III-nitrides semiconducting under hydrostatic pressure[7]. The pressure behavior of the energy band structures was discussed in the context of the postulated chemical trends in III-nitrides semiconductors. The total-energy calculations suggested that most of the nitrides under pressure transform to the semiconducting rocksalt phase. It was found that the transition pressures are 21.6 GPa, 16.6 GPa, and 850 GPa for InN, AlN, and BN, respectively. Experimental values that agree well with this have been found for the three compounds [7].

Indium nitride (InN) is a small band gap semiconductor material which has potential application in solar cells and high speed electronics.

The band gap of InN has now been established to be between 0.65 and 0.7 eV depending on temperature [8,9]. The effective electron mass ( $m^*$ ) of InN is between  $0.04m_0$  and  $0.07 m_0$ , which is the smallest effective electron mass among the nitrides but perhaps also of all semiconductors[10].

Recently, InN has attracted considerable attention due to its potential applications, which are suggested because of its superior transport properties on one side, and the seemingly conflicting results of various investigations, on the other side. The most important results were the repeated observations of an effective band gap of about 0.7 eV by optical techniques, in contrast to the value of 1.9 eV established for the last 20 years[11]. The growth of InN is very difficult due to the low dissociation temperature and the extremely high equilibrium vapor pressure of nitrogen. Nevertheless, in the last four years, considerable progress has been made to grow epitaxial hexagonal InN films by molecular beam epitaxial (MBE) and metal organic vapor phase epitaxy (MOVPE) [12, 13]. It was found that the hexagonal wurtzite phase with space group  $P6_3mc$  is the thermodynamically stable under ambient conditions, also, successful growth by MBE has been reported for cubic InN crystallizing in zinc-blende (ZB) structure with space group  $F43m$  [14,15]. Theoretical studies based on total-energy calculations clearly predict a first-order phase transformation from the wurtzite into the rock salt (RS) structure with space group  $Fm3m$  under hydrostatic pressure [16]. Theoretical studies of the atomic structures, in particular the lattice constants, were usually based

on the density functional theory (DFT) [17]. They give a unique picture if the In  $4d$  electrons are included in the calculations. Deviations arise mainly from the treatment of exchange and correlation (XC) within the local density approximation (LDA) or the generalized gradient approximation (GGA). Other small deviations are due to the treatment of the electron-ion interaction and the expansion of wave functions in a certain basis set. Much more confusing are the results of various theoretical studies. It is well known that the density functional theory in (LDA) or (GGA), which is widely used in modern band-structure calculations, severely underestimates the fundamental gaps and transition energies of semiconductors and insulators. For InN the DFT-LDA and DFT-GGA calculations usually give rise to negative energy gaps between 0.0 and -0.3 eV for wurtzite and somewhat more negative values for zinc blende if the In  $4d$  electrons are taken into account [15].

Aluminum nitride (AlN) has a hexagonal crystal structure called the wurtzite crystal structure (WZ), that has an extremely wide band gap (6.2 eV) semiconductor material. Also, it has a potential application for deep ultraviolet optoelectronics. Aluminum nitride is a mostly covalently bonded material. The space group for this structure is  $P6_3mc$  [18].

It was found that AlN is stable at very high temperatures in inert atmospheres. It refers to a gaseous mixture that contains little or no oxygen and primarily consists of non-reactive gases or gases that have a high threshold before they react. Nitrogen, argon, helium, and carbon dioxide are

common components of inert gas mixtures [18]. Currently, there is much research into developing light-emitting diodes to operate in the ultraviolet using the gallium nitride based semiconductors and alloy aluminum gallium nitride, wavelengths as short as 250 nm have been reported. In May 2006 an inefficient light emitting diode (LED) emission at 210 nm was reported[18]. The large band gap for AlN allows a wavelength of around 200 nm to be achieved, in principle. Therefore, AlN is the best material for constructing devices for the ultra violet region[19]. AlN, which has partially ionic and partially covalent chemical bonds, is an important coordinated III-nitrides compound. It has a high melting point, a high thermal conductivity, and a large bulk modulus. At ambient condition, AlN is generally reported to be no polymorphous, crystallizes in the wurtzite structure[24]. The cubic zincblende (ZB) form has also been theoretically reported to be metastable [19].

Besides important practical applications, AlN is also a unique semiconductor compound for fundamental studies. In contrast to all the other II–VI and III–V binary semiconductors, AlN in the zinc-blende structure has a larger band gap than that in the wurtzite structure. AlN is also the only WZ semiconductor compound that has been predicted to have a negative crystal field splitting at the top of valence band [20]. Confirmation of these predictions are important because the negative crystal field splitting can lead to unusual optical properties of AlN than other wurtzite semiconductors such as GaN [21]. The band structure and optical properties of AlN is very limited. For example, the detailed band

structure parameters near the G point of AlN are still unclear. The band gap was determined in the past only by optical absorption and transmission measurements with energy values scattered around 6.3 eV at liquid helium temperatures [22]. The band structure parameters of AlN, including the effective masses of electrons and holes as well as the character and splitting at the valence band edge are not yet well understood. Fundamental optical transitions including the band-to-band and excitonic transitions have not been well investigated. It is, therefore, of fundamental and technological importance to fill in the unknowns for AlN [23].

AlN is suitable for high-temperature electronics and opto-electronic applications. It was characterized by high temperature stability (melting temperature 3000 °C), high elastic stiffness and good thermal conductivity. AlN crystallizes in the WZ structure (WZ-AlN) is the only III –nitrides based Al semiconductor compound with a direct band gap. The zincblende structure form has been theoretically reported to be metastable [24,25], and only the calculated lattice parameter  $a = 4.37$  is available [26].

Both WZ-AlN and ZB-AlN have been the subject of extensive theoretical studies ranging from the semi-empirical to the first-principles methods within the density functional theory (DFT) framework using both pseudopotential and all-electron approaches[27,28].

Boron nitride (BN) is a binary chemical compound, consisting of equal numbers of boron and nitrogen atoms. Cubic boron nitride is an electrical insulator but an excellent conductor of heat. This diamond-like

polymorph, known as cubic boron nitride, is widely used as an abrasive for industrial tools. Its usefulness arises from its insolubility in iron, nickel, and related alloys at high temperatures, whereas diamond is soluble in these metals to give carbides. Like diamond, cubic BN has good thermal conductivity, caused by phonons. In contact with oxygen at high temperatures, BN forms a passivation layer of boron oxide. Boron nitride binds well with metals, due to formation of interlayers of metal borides or nitrides. Materials with cubic boron nitride crystals are often used in the tool bits of cutting tools. For grinding applications, softer binders (e.g, resin, porous ceramics, and soft metals) are used. Ceramic binders can be used as well [29].

Ab initio is a computational chemistry methods based on quantum chemistry. It indicates that the calculations of structural energies calculation is from first principles and that no empirical data is used [30]. Also, it indicates that cubic BN (ZB-BN) is the most stable structure at ambient conditions while the other structures are local energy minima with large energy barriers separating them[31]. These large energy barriers are responsible for the metastability of the other crystal structures. Despite the theoretical indication that (ZB-BN) is the most stable structure at ambient conditions, it is very difficult to grow high quality (ZB-BN) crystals. The hexagonal BN (WZ-BN) is the most common synthesized product. In fact, it was accepted for a long time that (WZ-BN) is the most stable structure at ambient conditions. But more recent experimental investigations and ab initio calculations affirm that (ZB-BN) is the most stable structure [32].

As mentioned earlier, there are some conflicts in the obtained results for AlN, InN, and BN compounds. The motivation beyond this study is to give a better understanding for the structural parameters, band structure and transition pressure for these compounds.

To obtain the goal of this study, the Full-Potential Linearized Augmented Plane Wave method as implemented by WIEN2K code (which is based on the density functional theory in the local density approximation and generalized gradient approximation is used). This method is an efficient and accurate approach for studying various properties of condensed matter system. So the aim of this study is to:

- 1) calculate the structural parameters (lattice parameters  $a$ , bulk modulus  $B$  and its derivative  $B'$ ) for ZB, RS phases of AlN, InN, and BN compounds; and WZ phase of AlN and InN compounds.
- 2) determine the equation of state of all previous phases for AlN, BN and InN compounds, by calculating the total energy at different volumes and fitting the calculated values to the Murnaghan's equation of state (EOS).
- 3) determine the transition pressure from ZB to RS for BN, WZ to ZB and WZ to RS for AlN and InN compounds.
- 4) determine the band structure of these phases for AlN, BN and InN compounds.

The present thesis is divided into four chapters. Chapter two presents the density functional theory, Kohn Sham equation, local density approximation, and generalized gradient approximation. Chapter three presents the computational details. Finally, chapter four presents the results and conclusions.

## Chapter 2

### Methodology

#### 2.1 Density Functional Theory

Physics and chemistry use a theory called Density functional theory (DFT), which is a quantum mechanical theory, to examine the electronic structure of many body systems, especially, atoms, molecules and the condensed phases. DFT is one of the most common and flexible technique obtainable in condensed matter physics, computational physics, and computational chemistry [33], due to its capability to deal with large numbers of electrons with complete precision [34].

Time-dependent density-functional theory (TDDFT) is the generalization of ground-state DFT to include time-dependent external potentials on electrons, and its formal validity was set up with the Runge-Gross theorem [35]. The analogous connection between time-dependent densities and time-dependent potentials for a given preliminary state guides to the time-dependent Kohn-Sham system, which is a set of non-interacting presumptive electrons moving in a time-dependent Kohn-Sham potentials. TDDFT has been applied to many problems in atomic, molecular and solid-state systems, including optical response, dynamic polarizabilities and hyperpolarizabilities, excitation energies, species in intense laser fields and highly energetic collisions [36].

The principle of DFT is to illustrate an interconnecting system of fermions by means of its density and not by its many-body wave function [37]. While DFT chiefly gives a good explanation and portrayal of ground state qualities. Practical applications of DFT rely on rough calculations for

the so-called exchange-correlation probability. The exchange-correlation probability portrays the influences of the Pauli principle and the Coulomb possibility beyond a pure electrostatic interaction of the electrons. The precise exchange-correlation probability gives a solution of the many-body problem precisely, which is obviously not possible in solids [37].

In spite of the fact that density functional theory has its theoretical roots in the Thomas-Fermi model, it was put on a solid hypothetical foundation by the two Hohenberg-Kohn theorems (H-K) [38]. The original H-K theorems held only for non-degenerate ground states in the absence of a magnetic field, although they have since been generalized to include them [39].

The ground state properties of a many-electron system are exclusively decided by an electron density that depends only on 3 spatial coordinates, this is shown in the first H-K theorem. It puts down the base work for reducing the many-body problem of  $N$  electrons with  $3N$  spatial coordinates to only 3 spatial coordinates, by the use of functional of the electron density. This theorem can be expanded to the time-dependent sphere to build up time-dependent density functional theory, which can be applied to portray stimulated conditions. The second H-K theorem defines an energy functional for the system and gives evidences to prove that the proper ground state electron density reduces this energy functional [33].

The intractable many-body problem of interacting electrons in a static external potential, within the framework of Kohn-Sham DFT(KS-DFT), is reduced to a tractable problem of non-interacting electrons

moving in an effectual potential. The effective potential contains the external potential and the effects of the Coulomb interactions between the electrons, e.g., the exchange and correlation interactions. Modeling the latter two interactions becomes the difficulty within KS DFT. The simplest rough calculation is the local-density approximation (LDA), which depends on precise exchange energy for a uniform electron gas, which can be obtained from the Thomas-Fermi model, and from fits to the correlation energy for a uniform electron gas.

Hohenberg and Kohn [38] were the first to formulate the special place of DFT in 1964 which becomes directly clear from the fundamentals, Here a derivation of DFT and its formula.

The nuclei of the treated molecules or clusters ,as usual in many-body electronic structure calculations, are seen as fixed (the Born-Oppenheimer approximation), generating a static external potential  $V$  in which the electrons are moving. A stationary electronic state is then portrayed by a wave function  $\Psi(\vec{r}_1, \dots, \vec{r}_N)$  satisfying the many-electron Schr dinger equation:

$$\hat{H}\Psi = [\hat{T} + \hat{V} + \hat{U}] \Psi = \left[ \sum_i^N -\frac{\hbar^2}{2m} \nabla_i^2 + \sum_i^N V(\vec{r}_i) + \sum_{i < j}^N U(\vec{r}_i, \vec{r}_j) \right] \Psi = E\Psi \quad (2-1)$$

where  $\hat{H}$  is the electronic molecular Hamiltonian,  $N$  is the number of electrons,  $\hat{T}$  is the  $N$ -electron kinetic energy,  $\hat{V}$  is the  $N$ -electron potential energy from the external field, and  $\hat{U}$  is the electron-electron interaction energy for the  $N$ -electron system. The operators  $\hat{T}$  and  $\hat{U}$  are

so-called universal operators as they are alike for any system, while  $\hat{V}$  is system dependent, i.e. non-universal. The differentiation between having separate single-particle problems and the much more complex many-particle problem stems from the interaction term  $\hat{U}$ .

The many-body Schrödinger equations solved by many complicated techniques based on the extension of the wave function in Slater determinants. While the easiest one is the Hartree-Fock technique, more sophisticated techniques are usually classified as post-Hartree-Fock techniques. However, the problem with these techniques is the vast computational effort, which makes it almost unfeasible to apply them competently to larger, more complicated systems.

Here DFT offers an attractive substitute, being much more adaptable as it provides a way to systematically map the many-body problem, with  $\hat{U}$ , onto a single-body problem without  $\hat{U}$ . In DFT the key changeable is the particle density  $n(\vec{r})$ , which for a normalized  $\Psi$  is given by:

$$n(\vec{r}) = N \int d^3 r_1 \int d^3 r_2 \dots \int d^3 r_N \Psi^*(\vec{r}_1, \vec{r}_2, \dots, \vec{r}_N) \Psi(\vec{r}_1, \vec{r}_2, \dots, \vec{r}_N) \quad (2-2)$$

This relation can be reversed, that is to say, for a given ground-state density  $n_0(\vec{r})$  it is principally potential, to work out the equivalent ground-state wave function  $\Psi_0(\vec{r}_1, \dots, \vec{r}_N)$ . That is to say,  $\Psi_0$  is a sole

functional of  $n_0$ ,  $\Psi_0 = \Psi[n_0]$  and as a result the ground-state expectation value of an observable  $\hat{O}$  is also a functional of  $n_0$

$$O[n_0] = \langle \Psi[n_0] | \hat{O} | \Psi[n_0] \rangle \quad (2-3)$$

In particular, the ground-state energy is a functional of  $n_0$

$$E_0 = E[n_0] = \langle \Psi[n_0] | \hat{T} + \hat{V} + \hat{U} | \Psi[n_0] \rangle \quad (2-4)$$

$$= \langle \Psi[n_0] | \hat{T} | \Psi[n_0] \rangle + \langle \Psi[n_0] | \hat{V} | \Psi[n_0] \rangle + \langle \Psi[n_0] | \hat{U} | \Psi[n_0] \rangle \quad (2-5)$$

$$= \hat{T}[n_0] + \hat{V}[n_0] + \hat{U}[n_0] \quad (2-6)$$

where the contribution of the external  $\langle \Psi[n_0] | \hat{V} | \Psi[n_0] \rangle$

potential can be written clearly in terms of the ground-state density  $n_0$

$$V[n_0] = \int V(\vec{r}) n_0(\vec{r}) d^3 r \quad (2-7)$$

More commonly, the contribution of the external potential  $\langle \Psi | \hat{V} | \Psi \rangle$  can be written clearly in terms of the density  $n$ ,

$$V[n] = \int V(\vec{r}) n(\vec{r}) d^3 r \quad (2-8)$$

As mentioned above, the functional  $T[n]$  and  $U[n]$  are called universal functional, whereas  $V[n]$  is called a non-universal functional, as it relies on the system under study. Having a definite system, i.e., having specified  $\hat{V}$ , one then has to reduce the functional

$$E[n] = T[n] + U[n] + \int V(\vec{r})n(\vec{r})d^3r \quad (2-9)$$

In regards to  $n(\vec{r})$ , taking for granted one has got dependable terms for  $T(n)$  and  $U(n)$ . A successful reduction of the energy functional will produce the ground-state density  $n_0$  and thus all other ground-state observables.

The Lagrangian technique of undetermined multipliers[39] can be applied to solve the variation problems of minimizing the energy functional  $E(n)$ . First, one takes into accounts an energy functional that doesn't clearly have an electron-electron interaction energy term,

$$E_s[n] = \langle \Psi_s[n] | \hat{T}_s + \hat{V}_s | \Psi_s[n] \rangle \quad (2-10)$$

where  $\hat{T}_s$  indicates the non-interacting kinetic energy and  $\hat{V}_s$  is an external effectual potential in which the particles are moving. clearly, if  $\hat{V}_s$  is  $n_s(\vec{r})=n(\vec{r})$  selected to be

$$\hat{V}_s = \hat{V} + \hat{U} + (\hat{T} - \hat{T}_s) \quad (2-11)$$

Consequently, one can solve the so-called Kohn-Sham equations of this assisting non-interacting system,

$$\left[ -\frac{\hbar^2}{2m} \nabla^2 + V_s(\vec{r}) \right] \phi_i(\vec{r}) = \epsilon_i \phi_i(\vec{r}) \quad (2-12)$$

which produces the  $\phi_i$  orbital that reproduce the density  $n(\vec{r})$  of the authentic many-body system

$$n(\vec{r}) = n_s(\vec{r}) = \sum_i^N |\phi_i(\vec{r})|^2 \quad (2-13)$$

The effective single-particle potential can be written in more detail as

$$V_s(\vec{r}) = V(\vec{r}) + \int \frac{e^2 n_s(\vec{r}')}{|\vec{r} - \vec{r}'|} d^3 r' + V_{XC}[n_s(\vec{r})] \quad (2-14)$$

where the second term stands for the so-called Hartree expression portraying the electron-electron Coulomb repulsion, while the last expression  $V_{XC}$  is called the exchange-correlation possibility. Here,  $V_{XC}$  has all the many-particle interactions. Since the Hartree expression and  $V_{XC}$  rely on  $n(\vec{r})$ , which relies on the  $\phi_i$ , which in turn relies on  $\hat{V}_s$ , the problem of solving the Kohn-Sham equation has to be done in a self-consistent way. One typically begins with an first guess for  $n(\vec{r})$ , then works out the equivalent  $\hat{V}_s$  and solves the Kohn-Sham equations for the  $\phi_i$  [33].

To conclude, techniques in DFT are complex and different, but can roughly be partitioned into three categories [40]:

- Techniques that apply a local density rough calculation (LDA). The LDA is decided exclusively and based on the qualities of the electron density. The significant supposition of this approximation is that, for a molecule with many electrons in a gaseous state, the density is consistent throughout the molecule. This is not the case for molecules, where the electron density is decidedly not consistent. This approximation does, however, work well with electronic band

structures of solids, which illustrates the scope of energies in which electrons are allowed or not allowed. Outside of these applications, however, LDA's are not very acceptable.

- Techniques that unite the electron density calculations with a gradient correction factor. A gradient in mathematics is a function that measures the rate of change of some property. In this case, the gradient seems to explain the non-uniformity of the electron density, and as such is known as gradient-corrected. Another expression for this is non-local.
- Techniques that are a mixture of a HF approximation to the exchange energy and a DFT approximation to the exchange energy, all united with a functional that has electron correlation. These Techniques are known as hybrid techniques, and are now the most common and popular DFT techniques used in practice.

## 2.2 Kohn Sham Equations

A set of eigen value equations within density functional theory (DFT) are called Kohn Sham equations. As mentioned above, DFT tries to minimize a many-body problem for the N particle wave function  $\Psi_0(\vec{r}_1, \dots, \vec{r}_N)$  to one in terms of the charge density  $n(\vec{r})$  which relies on 3 variables, using the Hohenberg-Kohn theorems[41]. The total energy  $E$  of the system as a functional of the charge density can be written as :

$$E(n) = T(n) + \int V_{ext}(r)n(r)dr + V_H[n] + E_{xc}[n] \quad (2-15)$$

where T is the kinetic energy of the system,  $V_{ext}$  is an external potential acting on the system, and

$$V_H = \frac{e^2}{2} \int \frac{n(r) n(r')}{|r-r'|} dr dr' \quad (2-16)$$

Is the Hartree energy and  $E_{xc}$  is the exchange-correlation energy.

The straight forward application of this formula has two barriers:

First, the exchange-correlation energy  $E_{xc}$  is not known precisely, and second, the kinetic term must be created in terms of the charge density. As was first suggested by Kohn and Sham, the charge density  $n(r)$  can be written as the sum of the squares of a set of orthonormal wave functions

$\phi_i(r)$ :

$$n(r) = \sum_i^N |\phi_i(r)|^2 \quad (2-17)$$

The unit of charge density  $n(r)$  is ( $c/m^3$ ).

Equation (2-17) represents the solution to the Schrödinger equation for  $N$  non-interacting electrons moving in an effectual potential  $V_{eff}(r)$

$$-\frac{\hbar^2}{2m} \nabla^2 \phi_i(r) + V_{eff}(r) \phi_i(r) = \varepsilon_i \phi_i(r) \quad (2-18)$$

where the effectual potential is defined to be

$$V_{eff}(r) = V_{ext}(r) + e^2 \int \frac{n(r')}{|r-r'|} dr' + \frac{\delta E_{xc}[n]}{\delta n} \quad (2-19)$$

These three equations form the Kohn-Sham orbital equations in their standard form. This system is then solved iteratively, until self-consistency is approached. Note that the eigen values  $\varepsilon_i$  have no physical meaning, only

the total sum, which matches the energy of the entire system  $E$  through the equation[42]:

$$E = \sum_i^N \varepsilon_i - V_H[n] + E_{xc}[n] - \int \frac{\delta E_{xc}[n]}{\delta n(r)} n(r) dr \quad (2-20)$$

Schematic representation of the self-consistent loop for solution of the Kohn-Sham equations. Generally speaking one must repeat two such circles at once for the two spins, with the potential for each spin relying upon the density of both spins [43].

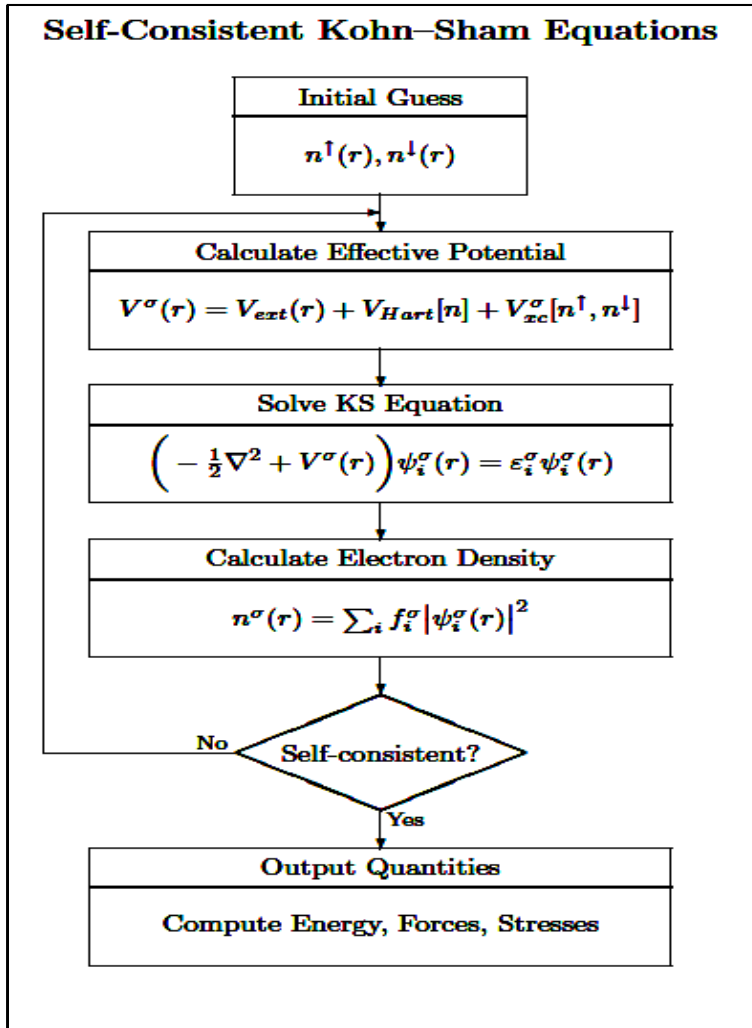


Figure (2.1): Flow chart of solving the self-consistent Kohn-Sham equation

Practically, there are several distinct ways in which Kohn-Sham theory can be applied depending on what is being examined. In solid state calculations, the local density approximations are still commonly used along with plane wave basis sets, as an electron gas approach is more suitable for electrons delocalized through an infinite solid. In molecular calculations, however, more complicated functionals are needed, and a huge variety of exchange-correlation functionals have been developed for chemical applications. Some of these are incompatible with the uniform electron gas approximation, however, they must reduce to LDA in the electron gas limit. For molecular applications, in particular for hybrid functionals, Kohn-Sham DFT techniques are usually applied just like Hartree-Fock itself [44].

The main difficulty with DFT is that the precise functionals for exchange and correlation are not identified except for the free electron gas. However, rough calculations exist which allow the calculation of certain physical amounts rather precisely. In physics the most widely used approximation is the local-density approximation (LDA).

### **2.3 Local Density Approximation**

One of the efficient rough calculation techniques for working out the exchange-correlation term in the density functional theory (DFT) is the local density approximation (LDA). LDA has widely been applied to portray a variety of close-ranged exchange-correlation interactions of, for instance, covalent bonding systems. However, LDA has serious limitations

that this approximation cannot provide estimation to the long-ranged exchange-correlation interaction, as typified by the Van der Waals (VdW) interaction. The VdW interaction is one of the long-ranged electronic interactions which mainly add to the first stage of the material reactions such as the chemical reaction, crystal growth and physical absorption. To assess the VdW interaction, many efforts have been devoted to develop useful calculating recipes for the non-local exchange-correlation term [45].

Kohn and Sham applied LDA approximation to DFT [41]. The Hohenberg-Kohn theorem states that the energy of the ground state of a system of electrons is a functional of the electronic density, especially, the exchange and correlation (XC) energy is also a functional of the density (this energy can be seen as the quantum part of the electron-electron interaction). This XC functional is not identified accurately and must be approximated [38]. LDA is the simplest approximation for this functional, it is local in the sense that the electron exchange and correlation energy at any point in space is a function of the electron density at that point only.

The XC functional is the total of a correlation functional and an exchange functional:

$$E_{xc} = E_x + E_c \quad (2-21)$$

LDA uses the exchange for the uniform electron gas of a density equal to the density at the point where the exchange is to be assessed:

$$E_{xc} = \int d^3r n(\vec{r}) \left( \frac{-3e^2}{4\pi} \right) (3\pi^2 n(\vec{r}))^{\frac{1}{3}} \quad (2-22)$$

In SI units,  $n(\vec{r})$  is the electron density per unit volume at the point  $\vec{r}$ ; and  $e$  is the charge of an electron [46].

While looking for the ways out to the system of Schrödinger equation:

$$E\psi(x) = -\frac{1}{2m}\nabla^2\psi(x) + V(x)\psi(x) \quad (2-23)$$

It is found that all amounts are represented as functional of the electronic  $\mathcal{E}_{xc}(r)$  charge density. The significant point that makes this system easier to solve (or more accurately, needs less computation) than, for instance the Hartree-Fock equations, is that the efficient possibility is local. Therefore there is no more complication added in solving Schrödinger equation than there is in the Hartree approximation. Of course, this is only true if the exchange-correlation energy can be portrayed as a function of the local charge density. A technique of doing so is known as the local density approximation (LDA) [41]. As mentioned above in LDA, the exchange-correlation energy of an electronic system is built by taking for granted that the exchange-correlation energy for each electron at a point  $\vec{r}$  in the electron gas is equal to the exchange-correlation energy for each electron in a identical electron gas that has the same electron density at the point  $\vec{r}$ . It follows that:

$$E_{xc} \left[ n(\vec{r}) \right] = \int \mathcal{E}_{xc}(n(\vec{r})) n(\vec{r}) dr \quad (2-24)$$

so that

$$\mu_{xc}(\vec{\mathbf{r}}) = \frac{\delta \left[ n(\vec{\mathbf{r}}) \varepsilon_{xc}(n(\vec{\mathbf{r}})) \right]}{\delta n(\vec{\mathbf{r}})} \quad (2-25)$$

with

$$\varepsilon_{xc}(n(\vec{\mathbf{r}})) = \varepsilon_{xc}^{\text{hom}}(n(\vec{\mathbf{r}})) \quad (2-26)$$

Where  $\varepsilon_{xc}^{\text{hom}}(n(\vec{\mathbf{r}}))$  is exchange-correlation energy in identical electron gas. Equation (2-26) is the supposition that the exchange-correlation energy is purely local. Several parameterizations for  $\varepsilon_{xc}^{\text{hom}}(n(\vec{\mathbf{r}}))$  exist, but the most commonly used is that of Perdew and Zunger [47]. This parameterisation is based on the quantum Monte Carlo calculations of Ceperley and Alder [48] on homogeneous electron gases at various densities. The parameterization uses interpolation formulas to link these precise outcomes for the exchange and correlation energy at many dissimilar densities.

Adjustment to the exchange-correlation energy because of the inhomogeneities in the electronic charge density about  $\vec{\mathbf{r}}$  are overlooked, in LDA,. Therefore, it may at first seem somewhat surprising that such calculations are so successful, when taking into account this inexact nature

of the approximation. This can be to some extent ascribed to the fact that LDA gives the accurate sum rule to the exchange-correlation hole. That is, there is a total electronic charge of one electron excluded from the vicinity of the electron at  $\vec{r}$ . Endeavors to improve on LDA, such as gradient extensions to correct for in-homogeneities do not seem to show any enhancement in results got by the simple LDA. One of the reasons for this failure is that the sum rule is not obeyed by the exchange-correlation hole.

The contributions of electron-electron interactions in  $N$ -electron systems are shown briefly in Figure (2.2). It demonstrates the conditional electron probability distributions  $n(r)$  of  $N-1$  electrons around an electron with given spin located at  $r = 0$ .

All electrons are dealt with as independent, in the Hartree approximation [49], Figure (2-2a), therefore is structureless. Figure (2-2b) stands for the Hartree-Fock approximation where the  $N$ -electron wave function reflects the Pauli exclusion principle. Around the electron at  $r = 0$ . The exchange hole can be seen where the density of spins equal to that of the central electron is reduced. Electrons with opposite spins are unchanged. In the LDA (Figure (2-2c)), where spin states are degenerate, each sort of electron sees the same exchange-correlation hole (the sum rule being demonstrated where the size of the hole is one electron).

Figure (2-2d) shows electron-electron interaction for non-degenerate spin systems (the local spin density approximation (LSDA)). It can be seen that the spin degenerate LDA is basically the average of the LSDA.

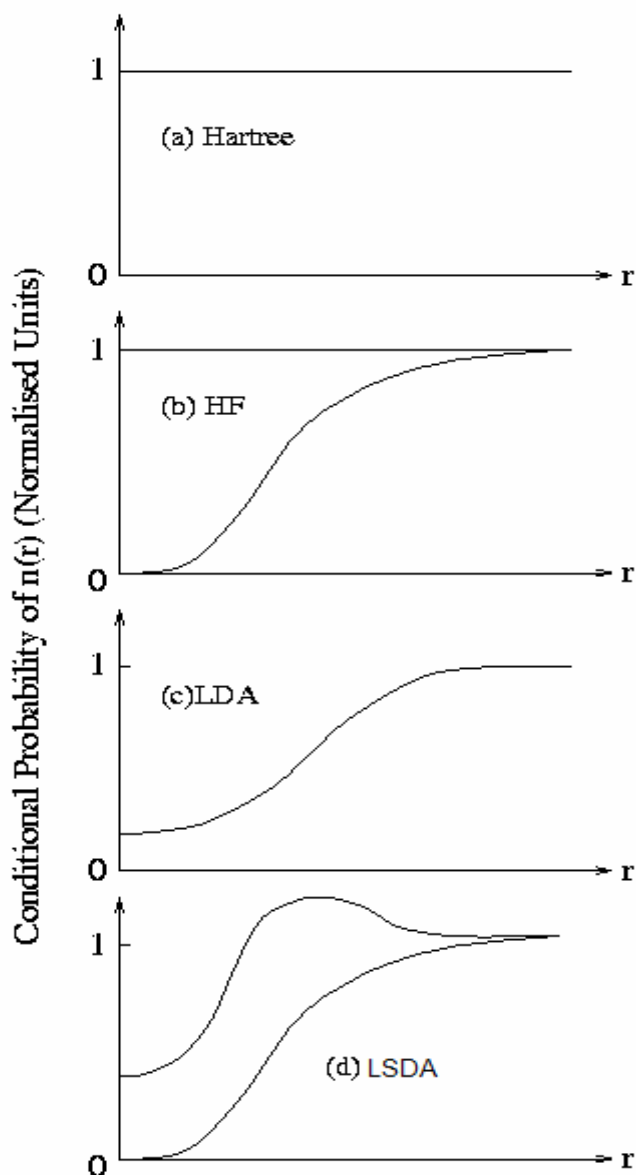


**Figure (2.2): Summary of the electron-electron interactions (excluding coulomb effects) in (a) the Hartree approximation, (b) the Hartree-Fock approximation, (c) the local density approximation and (d) the local spin density approximation which allows for different interactions for like-unlike spins.**

GGA's approximation has minimized the LDA errors of atomization energies of standard set of small molecules. This enhanced precision has made DFT an important element of quantum chemistry.

## 2.4 Generalized Gradient Approximation (GGA)

The local spin density (LSD) approximation has been the basis of electronic structure calculations in solid-state physics for many years [41]. This rough calculation may be written as:

$$E_{xc}^{LSD}(n_{\uparrow}, n_{\downarrow}) = \int d^3r n(\vec{r}) \varepsilon_{xc}^{unif} \left[ n_{\uparrow}(\vec{r}), n_{\downarrow}(\vec{r}) \right] \quad (2-27)$$

$\varepsilon_{xc}^{unif}(n_{\uparrow}, n_{\downarrow})$  exchange-correlation energy for each particle of a uniform electron gas [50]. The LSD exchange-correlation energies are inadequately negative (by about 10%) for almost all atoms, molecules, and solids. The LSD is a dependable, moderate-accuracy approximation. For many solid-state objectives, the LSD level of precision is adequate, but LSD is not precise enough for most chemical applications, which need the determination of energy diversities with substantial accuracy. Hence the disinterest of the quantum chemistry community toward density functional techniques until recently[51]. New gradient-corrected functional of the form:

$$E_{xc}^{GGA}[n_{\uparrow}, n_{\downarrow}] = \int d^3r f(n_{\uparrow}(\vec{r}), n_{\downarrow}(\vec{r}), \nabla n_{\uparrow}, \nabla n_{\downarrow}) \quad (2-28)$$

where  $f$  are functionals for different energies of the same system. These functionals may be partitioned into two wide categories: “locally based” functional, whose construction starts from the uniform electron gas, and "semi empirical" functional, which has one or more parameters fitted to

a particular finite system, which have minimized LSD atomization energy errors by about a factor of 5[52]. The generalized gradient approximation (GGA) has attracted much attention for its abstract simplicity and moderate computational workloads. at present, two GGA functional, one suggested by Becke and Perdew (BP)] and one suggested more recently by Perdew and Wang (PW), are the most popular ones in the literature [53]. Many calculations assessing the accuracy of the GGA have been reported and commonly demonstrate that the GGA substantially corrects the LDA error in the cohesive energies of molecules and solids[54]. Generalized gradient approximations (GGA's) to the exchange-correlation (XC) energy in density-functional theory, are at present receiving increasing attention as a straightforward substitute to improve over the local-density approximation (LDA) in ab initio total-energy calculations [50]. In a variety of fields , the GGA provided evidence to be more suitable than the LDA:

- (1) Binding energies of molecules and solids became more precise, correcting the trend of the LDA to over binding [55].
- (2) Activation energy obstacles, e.g., for the dissociate adsorption of H<sub>2</sub> on metal and semiconductor surfaces, are in distinctly better accordance with experiment. Reaction and activation energies for a variety of chemical reactions give the same enhancement [56].
- (3) The relative constancy of structural phases seems to be anticipated more realistically for magnetic and for nonmagnetic materials ,too [57].

Bulk structural qualities are often not developed within the GGA. While the lattice parameters always rise in comparison with the LDA, a closer agreement with experimental data is reported for alkali metals, 3 *d* metals, and some 4*d* metals. However, an overestimation of up to several percent is found for 5*d* metals and common semiconductors, their bulk moduli accordingly turning out to be too small (typically by  $\leq 25\%$ )[58].

## **2.5 The full-potential linearized augmented-plane wave technique**

The full-potential linearized augmented-plane wave (FP-LAPW) technique is well known to allow most precise calculation of the electronic structure and magnetic qualities of crystals and surfaces. The application of atomic forces has greatly maximized its applicability, but it is still commonly supposed that FP-LAPW computations need considerable higher computational effort in comparison with the pseudopotential plane wave (PPW) based techniques [59].

FP-LAPW has recently showed important progress. For example, researchers habitually work out magnetism and nuclear quantities (for example, isomer shifts, hyperfine fields, electric field gradients, and core level shifts) [60]. Also, forces and molecular dynamics have been applied, and recent optimizations have decreased the CPU time of FP-LAPW calculations significantly [59]. Nevertheless, because the computational expense and memory requirements are still fairly high, FP-LAPW implementations are suitable only to fairly complicated systems. One successful implementation of the FP-LAPW technique is the program

package WIEN2K, a code enhanced by Blaha, Schwarz and coworkers [61]. It has been successfully implemented to a various scope of difficulties such as electric field gradients [62] and systems such as high-temperature superconductors, minerals [63], surfaces of transition metals [64], or anti-ferromagnetic oxides [65] and even molecules [66]. Reducing the total energy of a system by comforting the atomic counterparts for complicated systems became potential by the application of atomic forces, and even molecular dynamics became possible. So far the main disadvantage of the FP-LAPW-technique in comparison with the pseudopotential plane-wave (PPW) [67] method has been its higher computational expense. This may be largely because of an inconsistency in optimization efforts spent on both techniques, and so we have investigated the FP-LAPW technique from a computational arithmetical viewpoint.

Lately, the development of the Augmented Plane Wave (APW) techniques from Slater's APW, to LAPW and the new APW+lo was portrayed by Schwarz et al[68].

One of the most precise techniques for performing electronic structure calculations for crystals is the full potential linearized augmented plane wave FP-LAPW technique. It is based on the density functional theory for the handling of exchange and correlation and uses (for example, the local spin density approximation) (LSDA). Effects, for valence states relativistic ,can be incorporated either in a scalar relativistic handling or

with the second dissimilarity technique including spin-orbit coupling. Core states are treated fully relativistically.

The FP- LAPW technique ,which is Like most ``energy-band techniques ,is a process for solving the Kohn-Sham equations for the ground state density, total energy, and (Kohn-Sham) eigen values (energy bands) of a many-electron system by presenting a basis set which is particularly modified to the problem.

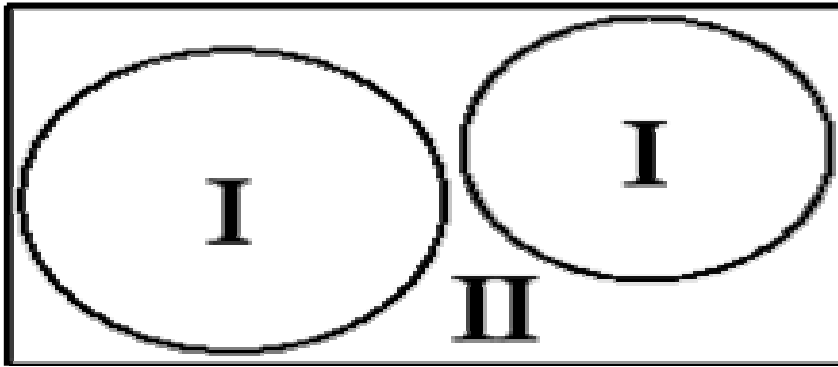


**Figure (2.3): Partitioning of the unit cell into atomic spheres (I) and an interstitial region (II)**

This alteration is achieved by partitioning the unit cell into (I) non-overlapping atomic circles (centered at the atomic sites) and (II) an interstitial region, that's to say, a region between two spaces. In the two sorts of regions diverse basis sets are used:

- Inside atomic sphere  $\mathbf{t}$  of radius  $\mathbf{R}_t$  a linear combination of radial functions times spherical harmonics  $\mathbf{Y}_{lm}(\mathbf{r})$  is used

$$\phi_{kn} = \sum_{lm} [A_{lm} u_l(\vec{\mathbf{r}}, E_l) + B_{lm} \dot{u}_l(\vec{\mathbf{r}}, E_l)] Y_{lm}(\vec{\mathbf{r}}) \quad (2-29)$$

where  $u_1(r, E_1)$  is the (at the origin) normal way out of the radial Schrödinger equation for energy  $E_1$  and the spherical part of the potential inside sphere,  $\dot{u}_l(r, E_l)$  is the energy derived of  $u_1$  taken at the similar energy. A linear mixture of these two functions comprise the linearization of the radial function; the coefficients  $A_{lm}$  and  $B_{lm}$  are functions of  $k_n$  decided by requiring that this root function  $\dot{u}_l$  goes with the equivalent basis function of the interstitial region;  $u_l$  and are achieved by numerical integration of the radial Schrödinger equation on a radial mesh inside the sphere.

- (II) in the interstitial zone a plane wave extension is applied

$$\phi_{k_n} = \frac{1}{\sqrt{w}} e^{ik_n r} \quad (2-30)$$

- where  $k_n = k + k_n$ ,  $k_n$  are the mutual lattice vectors and  $k$  is the wave vector inside the first Brillouin zone. Each plane wave is increased by an atomic-like function in every atomic sphere.

The solutions to the Kohn-Sham equations are extended in this joint basis set of LAPW's according to the linear dissimilarity technique

$$\psi_k = \sum_n c_n \phi_{k_n} \quad (2-31)$$

and the coefficients  $c_n$  are decided by the Rayleigh-Ritz variation rule. The union of this basis set is controlled by a disconnected

parameter  $R_{mt} K_{\max} = 6 - 9$ , where  $R_{mt}$  is the smallest atomic sphere radius in the unit cell and  $K_{\max}$  is the magnitude of the largest  $K$  vector.

Additional ( $K_n$  independent) basis functions can be added to improve upon the linearization and to make possible a reliable treatment of semi core and valence states in one energy window. They are called "local orbitals" and consist of a linear combination of 2 radial functions at 2 dissimilar energies and one energy derivative:

$$\phi_{lm}^{LO} = [A_{lm} u_l(\vec{r}, E_{1,l}) + B_{lm} \dot{u}_l(\vec{r}, E_{1,l}) + C_{lm} u_l(\vec{r}, E_{2,l})] Y_{lm}(\hat{r}) \quad (2-32)$$

The coefficients  $A_{lm}$ ,  $B_{lm}$ , and  $C_{lm}$ , are decided by the necessities that  $\phi^{LO}$  should be regularized and has zero value and slope at the sphere border.

The FP- LAPW technique, in its general form, extends the potential in the following form

$$V(\vec{r}) = \begin{cases} \sum_{lm} V_{lm}(\vec{r}) Y_{lm}(\hat{r}) & \text{insidesphere} \\ \sum_K V_K e^{iKr} & \text{outsidesphere} \end{cases} \quad (2-33)$$

And the charge densities analogously. Thus no form of rough calculations are made, a process often called the "full-potential" technique.

The "muffin-tin" rough calculation applied in early band calculations matches to keeping only the  $L=0$  and  $M=0$  component in the initial idiom of final equation. and only the  $K=0$  constituent in the second. This process matches to take the spherical rate inside the spheres and the volume rate in the interstitial region.

The entire energy is calculated according to Weinert *et al* [69].

The forces at the atoms are worked out according to Yu *et al* [70].

The Fermi energy and the weights of each band state can be worked out using an adapted tetrahedron (having four surfaces) technique [71].

## CHAPTER 3

### Computational Details

#### 3.1 Wurtzite Structure (WZ)

The wurtzite structure WZ has a hexagonal unit cell with two lattice parameters  $a$  and  $c$  in ratio  $c/a = 1.633$ . This structure is composed of two hexagonal closed-packed (hcp) sub lattices.

The primitive unit cell of the WZ structure is shown in Figure (3.1), while its conventional unit cell is shown in Figure (3.2). The conventional unit cell of WZ structure has a hcp lattice with two basis: Al, B or In atom at  $(a/3, 2a/3, 0)$  and N atom at  $(a/3, 2a/3, u)$ , where  $u$  is called the dimensionless cell internal structure parameter and  $a$  is the lattice parameters. The wurzite structure space group is  $p6_3mc$ .

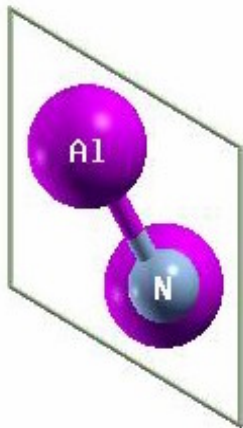
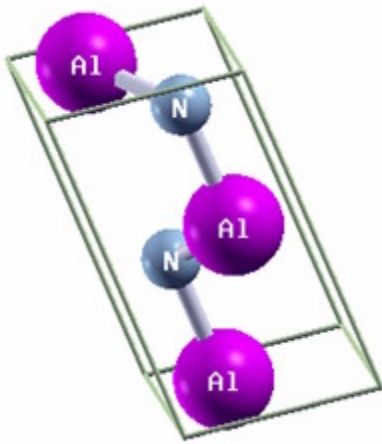


Figure (3.1): The primitive unit cell of AlN in wurtzite structure



**Figure (3.2): The conventional unit cell of AlN in the wurtzite structure**

### 3.2 Rocksalt Structure (RS)

In rocksalt (RS) structure the anions form a face-centered cubic (fcc) lattice where open sites are occupied by cations. The space group for the rocksalt structure is  $Fm\bar{3}m$ . The primitive unit cell of the RS structure is shown in Figure (3.3), while its conventional unit cell is shown in Figure (3.4). The coordinate of Al, B, or In atom is  $(0a, 0a, 0a)$  and the N atom at  $(a/2, a/2, a/2)$ .

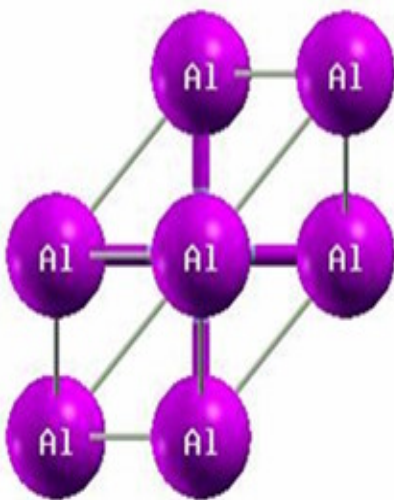


**Figure (3.3): The primitive unit cell of AlN in rocksalt structure**

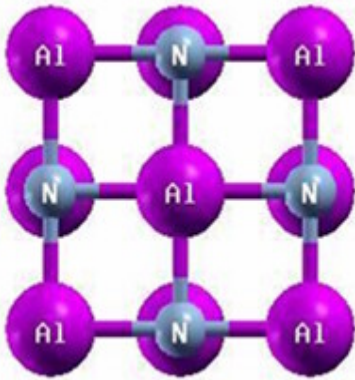


**Figure (3.4): Te conventional unit cell of AlN in the rocksalt structure**

### **3.3 Zincblende Structure (ZB)**

In semiconductors the most ambient-pressure structure is the Zincblende (ZB) structure. ZB structure is cubic with space group  $F43m$ . The Zincblende structure is also basically just an fcc lattice with two atoms at each lattice site. One atom centered at the lattice site itself and another atom offset from the lattice site by  $a/4$  along all axes[72]. The primitive unit cell of the ZB structure is shown in Figure (3.5), while its conventional unit cell is shown in Figure (3.6).

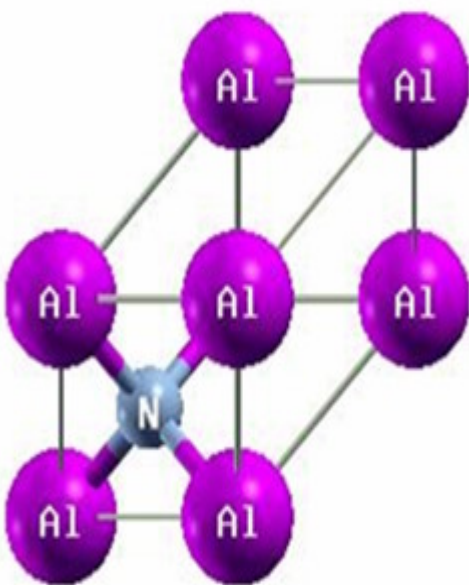


**Figure (3.5): The primitive unit cell of AlN in zincblende structure**

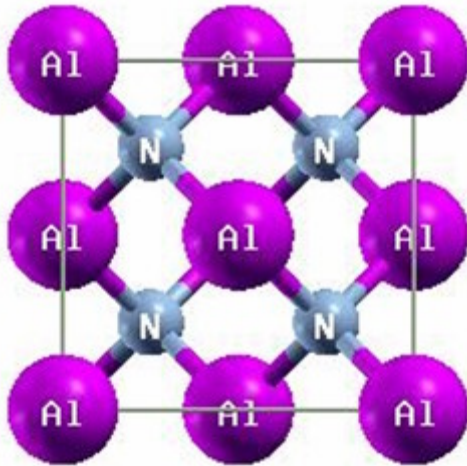


**Figure (3.6):** Te conventional unit cell of AlN in the zincblende structure

### 3.4 The Computational Details

In our calculations, we use the full-potential linearized augmented plane wave method (FP-LAPW) within the local density approximation (LDA) and the generalized gradient approximation (GGA) as implemented by WEIN2K code [73]. The FP-LAPW method is used to calculate the electronic and structural properties of AlN, BN, and InN in the Wurtzite, Zincblende, and Rocksalt phases.

As mentioned before the crystal structure of the ZB and RS phases can be defined by the lattice parameter  $a$ . The wurtzite structure, however is hexagonal structure, which depends on three structure parameters :  $a$ ,  $c$  and internal parameter,  $u$ . To determine the equilibrium geometry of wurzite phase we follow the following steps. In the first step the optimum value of  $u$  is determined by calculating total energies of  $c/a$  ratio. Then the equilibrium value and bulk modulus were determined by calculating the total energies for a set of volumes and fitting these to the Murnaghan's

equation of state [74]. The next step is calculating the total energies for 6 different values of  $c/a$ . After this step we find the minimum energy by fitting the resulting values to a parabola. Fixing the optimum value of  $a$  and  $c/a$ , we vary the parameter  $u$  and find the new total energy. Finally, with  $c/a$  and  $u$  fixed at their optimized value, we vary  $a$  and calculate the total energy at 6 different volumes, which we fit again by the Murnaghan's equation of state.

Before we start these calculations on WEIN2K code, a well known compound TiC is practiced. Inserting the lattice parameter  $a$ , the muffin-tin (MT) radius  $R_{MT}$ , and the atom's positions. We obtained structural parameters (bulk modulus  $B$ , the derivative of bulk modulus to pressure  $B'$  and the energy  $E$ ). We got results similar to published ones.

In our calculations we take the L-expansion of the non spherical potential and charge density  $L_{max}$  to be 12, according to convergent test, which shows that this value is the suitable one in our calculations, as shown in Figure 3.10.

**Table (3.1): L- expansion of the non spherical potential and energy using GGA and LDA approximations for RS-AlN.**

<b>L</b>	<b>Energy (Rydberg) (GGA)</b>	<b>Energy (Rydberg) (LDA)</b>
4	595.3579	592.83169
6	595.3394	592.82991
8	595.3379	592.82979
10	595.3378	592.82978
12	595.3378	592.82978

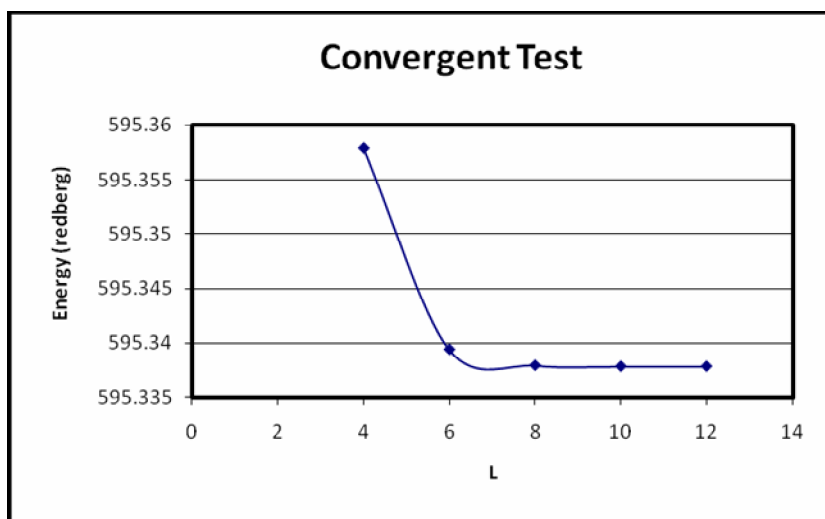


**Figure (3.7):** The convergent test using GGA approximation for RS-AlN.

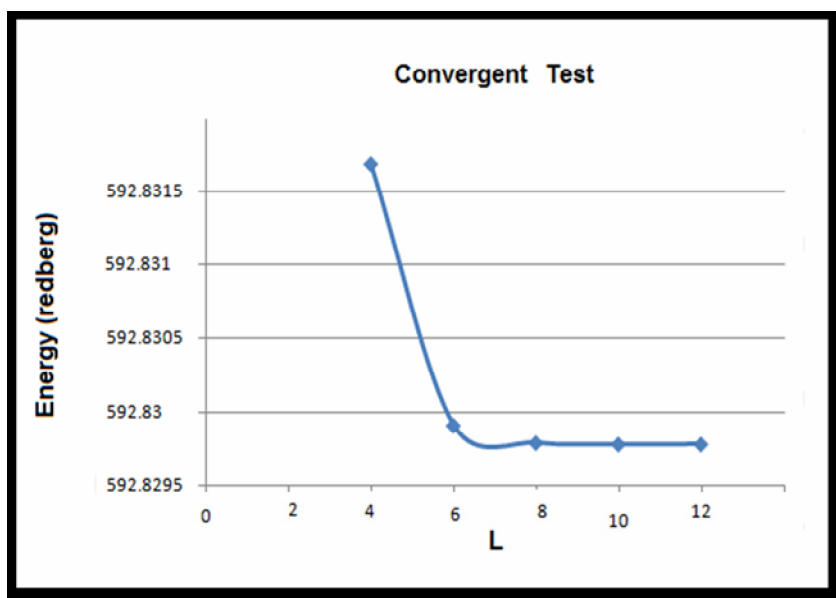


**Figure (3.8):** The convergent test using LDA approximation for RS-AlN.

For AlN compound the muffin-tin radius  $R_{MT}$  in ZB, RS, and WZ structure are taken to be 1.9 and 1.5 for Al and N, respectively, in GGA calculation ; whereas the  $R_{MT}$  are taken to be 1.6 and 1.6 for Al and N, respectively in LDA calculation. It is found that in the MT spheres, the L-expansion of the nonspherical potential and charge density was carried out up to  $L_{max} = 12$ . In order to achieve energy eigenvalue convergence, it is expanded the basis function up to  $R_{MT}K_{MAX} = 10$  (where

$K_{MAX}$  is the maximum modulus for the reciprocal lattice vector, and  $R_{MT}$  is the average radius of the MT spheres), equivalent to approximately 1400 and 300 basis functions per atom for WZ and cubic phases, respectively. The  $k$  integration over the Brillouin zone is performed up to a  $4 \times 4 \times 4$  Monkhorst–Pack [75] mesh. The number of sampling  $k$ -points in the irreducible Brillouin Zone is 114, 72 and 72 for the WZ , ZB and RS structures respectively, which correspond to  $12 \times 12 \times 12$   $k$ -points meshes for ZB and RS structures and to  $12 \times 12 \times 6$   $k$ -points for the WZ structure in LDA calculations, whereas the number of sampling  $k$ -points in the irreducible Brillouin Zone is 297, 165 and 165 for the WZ , ZB and RS structures respectively, which correspond to  $17 \times 17 \times 17$   $k$ -points meshes for ZB and RS structures and to  $17 \times 17 \times 9$   $k$ -points for the WZ structure in GGA calculations.

For BN compound the muffin –tin radius  $R_{MT}$  in ZB, RS structure is taken to be 1.25 for B and 1.25 for N in GGA calculation, whereas the  $R_{MT}$  in ZB, RS structure is taken to be 1.4 for B and 1.5 for N in LDA calculation. The number of sampling  $k$ -points in the irreducible Brillouin Zone is 5 for the ZB and RS structures respectively, which correspond to  $3 \times 3 \times 3$   $k$ -points meshes for ZB and RS structures in LDA calculations, whereas the number of sampling  $k$ -points in the irreducible Brillouin Zone is 14 for the ZB and RS structures respectively, which correspond to  $5 \times 5 \times 5$   $k$ -points meshes for ZB and RS structures in GGA calculations.

For InN Compound the muffin-tin radius  $R_{MT}$  in WZ, ZB, RS structures are taken to be 2.3 and 1.6 for In and N, respectively, in GGA calculation ; while the  $R_{MT}$  in WZ, ZB, and RS are taken to be 2.3 , 1.6 for In and N, respectively, in LDA calculation. The number of sampling k-points in the irreducible Brillouin Zone is 21, 10 and 10 for the WZ, ZB and RS structures respectively, which correspond to 4x4x4 k-points meshes for ZB and RS structures and to 6x6x3 k-points for the WZ structure in LDA and GGA calculations. In the case of the fcc Bravais lattice, an equidistant 8x8x8 mesh has been used; whereas in the case of the hexagonal Bravais lattice, we applied a 25x25x16 mesh [76].

## Chapter 4

### Results And Discussion

#### 4.1 AlN Compound:

AlN is a ceramic and refractory material and has combination of attractive physical properties such as : low thermal expansion, high thermal conductivity, high hardness and high melting points. In this section we present structural properties, band structure and transition pressure for AlN compound.

##### 4.1.1 Structural properties:

The structural parameters have been obtained by minimizing the total energy with respect to the volume and fitting it to the Murnaghan equation of state:

$$E(V) - E(V_0) = \frac{B_0 \cdot V}{B'_0} \left[ \frac{(V_0/V)B'_0}{B'_0 - 1} + 1 \right] - \frac{B_0 V}{B'_0 - 1} \quad (4-1)$$

where  $E(V)$  is the DFT ground-state energy with the cell volume  $V$ ,  $V_0$  is the unit-cell volume at zero pressure,  $B_0$  denotes the bulk modulus, and their first pressure derivative is [74]:

$$B'_0 = dB_0/dP \quad \text{at } P = 0 \quad (4-2)$$

The calculated lattice parameters for AlN, BN, and InN in LDA and GGA calculations are shown in Tables 4.1 and 4.2, respectively.

**Table (4.1): The calculated lattice parameters for AlN, BN, and InN using LDA method.**

Structure	AlN	BN	InN
ZB	a=4.349	3.615	4.96
RS	a=4.01	3.503	4.63
WZ	a=3.11 c=4.97 u=0.380		3.52 5.702 0.375

**Table (4.2): The calculated lattice parameters for AlN, BN, InN using GGA method.**

Structure	AlN	BN	InN
ZB	a=4.409	3.615	5.04
RS	a=4.07	3.503	4.71
WZ	a=3.113 c=5.023 u=0.380		3.58 5.7638 0.379

#### 4.1.1.a Wurtzite –AlN structure:

**Table (4.3): The structural parameters for wurtzite-AlN structure using LDA and GGA methods.**

Method		LDA	GGA	Experimental Results
a ( )	Present	3.0906	3.138	
	Other	3.057 <sup>a</sup> - 4.114 <sup>a</sup>	3.135 <sup>b</sup>	3.11 <sup>c</sup>
c ( )	Present	4.9449	5.024	
	Other	4.943 <sup>a</sup> - 5.046 <sup>a</sup>	5.023 <sup>b</sup>	4.978 <sup>c</sup>
c/a	Present	1.60	1.601	
	Other	1.604 <sup>a</sup> - 1.619 <sup>a</sup>	1.601 <sup>b</sup>	1.601 <sup>c</sup>
u	Present	0.380	0.380	
	Other	0.380 <sup>a</sup> - 0.383 <sup>a</sup>	0.3801 <sup>b</sup>	0.385 <sup>c</sup>
B <sub>o</sub> (GPa)	Present	211.0047	195.0232	
	Other	215 <sup>a</sup>	192.35 <sup>b</sup>	185 <sup>c</sup> - 212 <sup>c</sup>
B <sub>o</sub> <sup>/</sup> (GPa)	Present	3.8757	4.0295	
	Other	3.82 <sup>a</sup>	3.757 <sup>b</sup>	5.7 <sup>c</sup> - 6.3 <sup>c</sup>

<sup>a</sup>Ref.[77], <sup>b</sup> Ref.[78], <sup>c</sup> Ref.[79].

In table (4.3) we present structural properties (lattice constants  $a$ , bulk modulus  $B_0$  and  $B_0'$ ) for wurzite AlN in LDA and GGA calculations. As shown in this table the lattice constants ( $a$ ,  $c$ ) for the WZ-AlN used in our calculation are so closed to the experimental values.

For WZ-AlN the lattice parameters ( $a=3.08$  ,  $c=4.94$  ) determined by Wright and Nelson [80] using pseudopotential calculations, which is close to that obtained by us.

These parameters are slightly underestimated compared to the experimental values using the LDA method. Figure 4.1 shows the fitted total energy versus volume for WZ-AlN using GGA method, while Figure 4.2 shows the fitted total energy versus volume for WZ-AlN using LDA method.

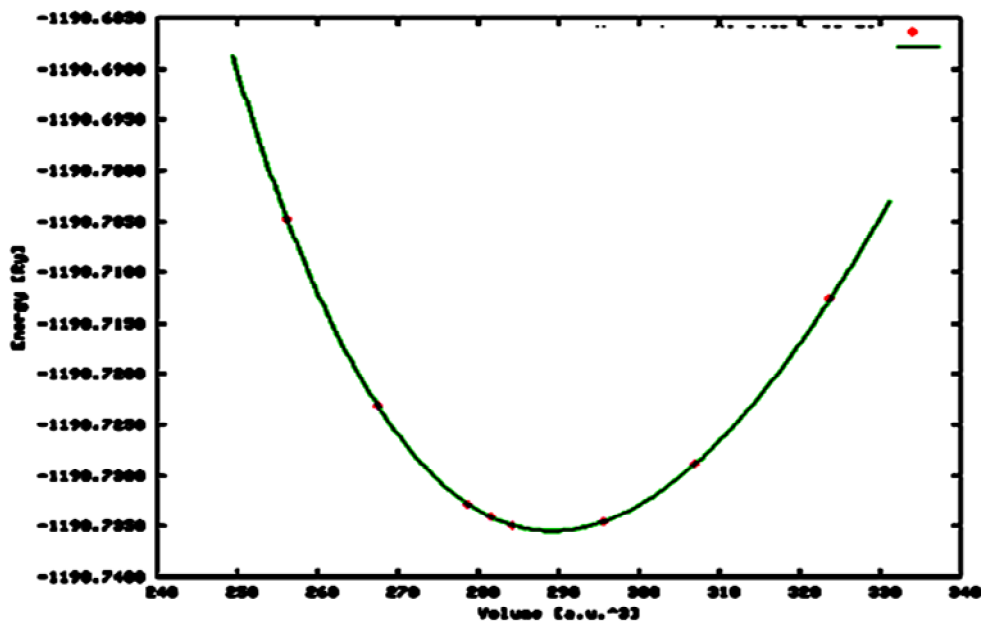


Figure (4.1): Energy versus volume for WZ-AlN using GGA method.

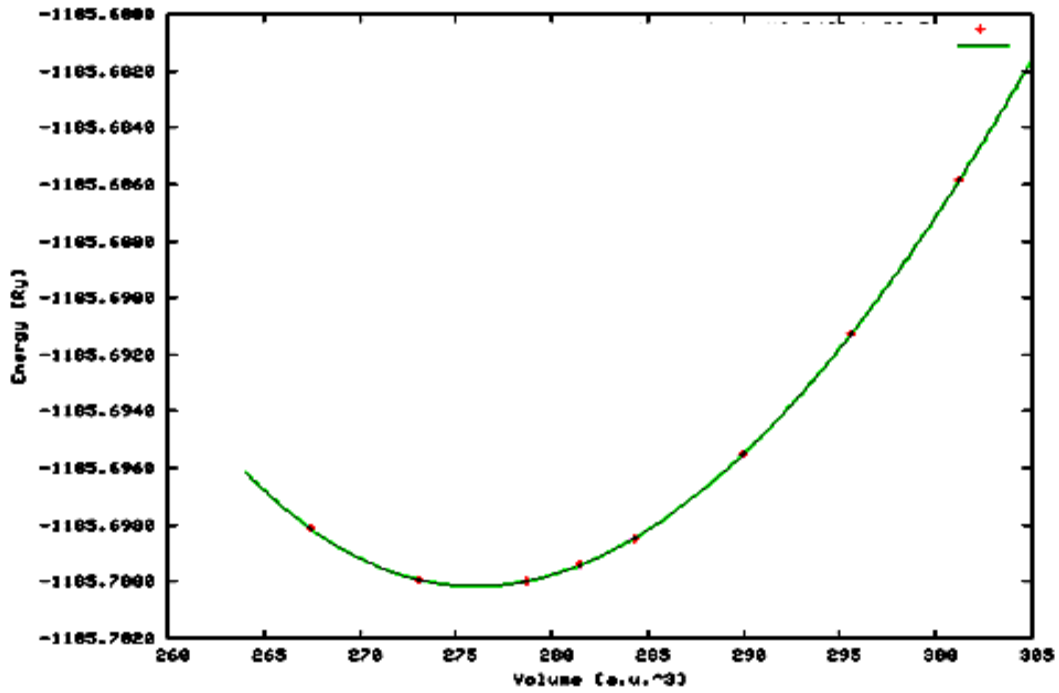


Figure (4.2) : Energy versus volume for WZ-AlN using LDA method.

#### 4.1.1.b Zincblende –AlN structure:

Table (4.4): The structural parameters for zincblende-AlN structure using LDA and GGA Methods.

Method	a ( )		Experimental Results	B (GPa)		B' (GPa)	
	Present	Other		Present	Other	Present	Other
LDA	4.344	4.31 <sup>e</sup>	4.38 <sup>c</sup>	209.191	213 <sup>e</sup>	3.927	3.2 <sup>e</sup>
			4.37 <sup>d</sup>				
GGA	4.41	4.39 <sup>f</sup>		193.715	191 <sup>f</sup>	4.0899	3.81 <sup>f</sup>

<sup>c</sup>Ref.[79], <sup>d</sup>Ref.[26], <sup>e</sup>Ref.[ 81], <sup>f</sup>Ref.[82].

In table 4.4, it is shown that the lattice constant  $a$  ( ) for the ZB-AlN in LDA method is underestimated compared to the experimental value, but in GGA method is overestimated compared to the experimental value. Also, in GGA method our calculation is in better agreement compared to the others. In Figure 4.3 shows the fitted total energy versus volume for ZB-AlN using GGA method, while Figure 4.4 shows the fitted total energy versus volume for ZB-AlN using LDA method.

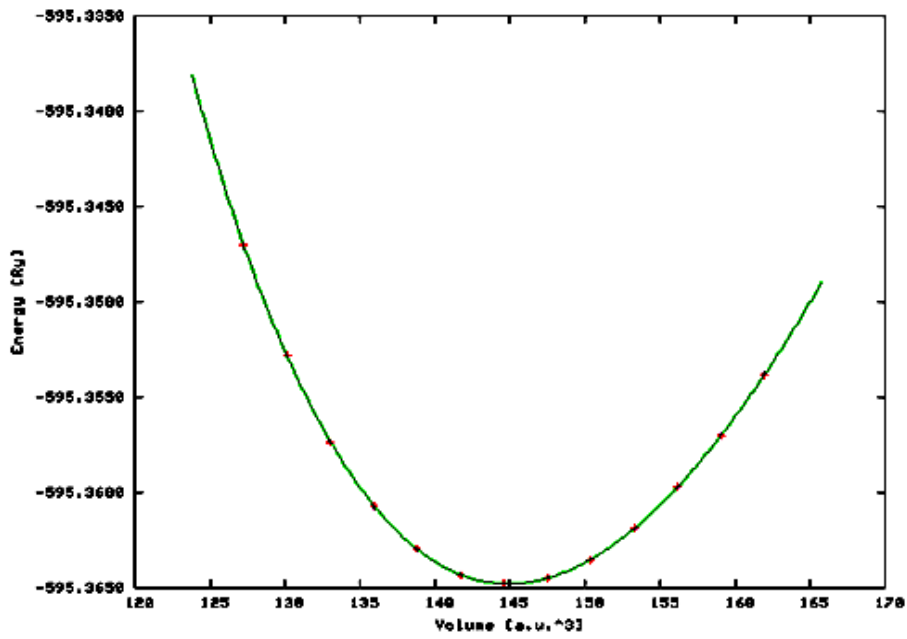


Figure (4.3): Energy versus volume for ZB-AlN using GGA method.

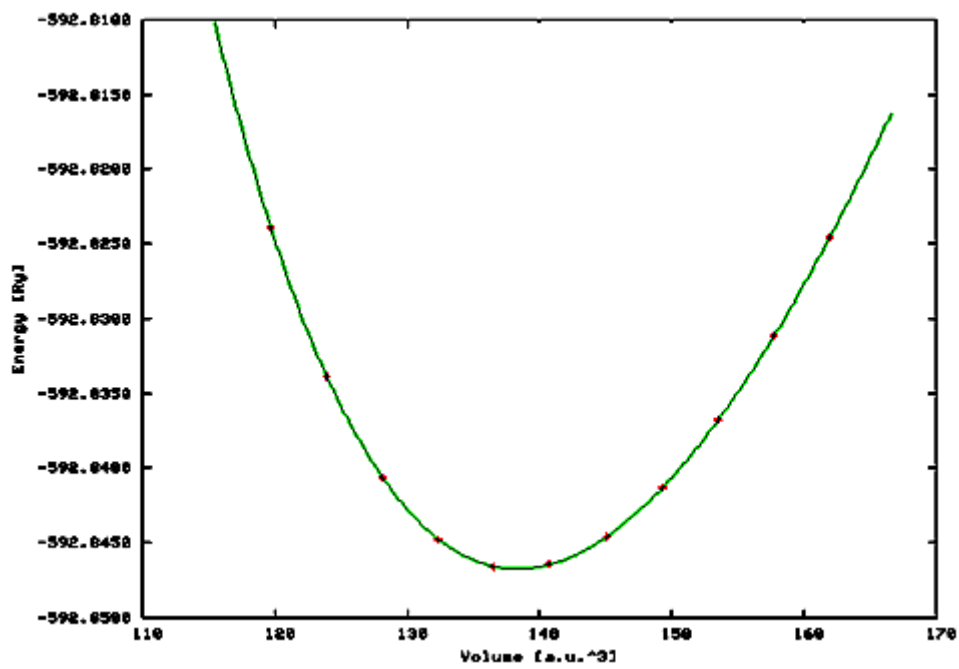


Figure (4.4): Energy versus volume for ZB-AlN using LDA method.

### 4.1.1.c Rocksalt- AlN structure:

**Table (4.5): The structural parameters for rocksalt-AlN structure using LDA and GGA methods.**

Method	a ( )		B <sub>0</sub> (GPa)		B <sub>0</sub> ' (GPa)		Experimental Results
	Present	Other	Present	Other	Present	Other	
							a = 4.045 <sup>j</sup>
LDA	4.012	3.978 <sup>g</sup>	273.9226	272 <sup>g</sup>	3.9958	3.8 <sup>g</sup>	B <sub>0</sub> = 221 <sup>i</sup>
GGA	4.076	4.074 <sup>h</sup>	249.0913	252 <sup>h</sup>	3.9822	3.901 <sup>h</sup>	B <sub>0</sub> ' = 4.8 <sup>i</sup>

<sup>g</sup>Ref.[83], <sup>h</sup> Ref.[1], <sup>i</sup> Ref.[84], <sup>j</sup> Ref.[85]

In table 4.5, we notice that the lattice constant in LDA method is underestimated, while in GGA method is overestimated compared to the experimental value. The Bulk modulus obtained in LDA method is larger than both GGA and experimental values.

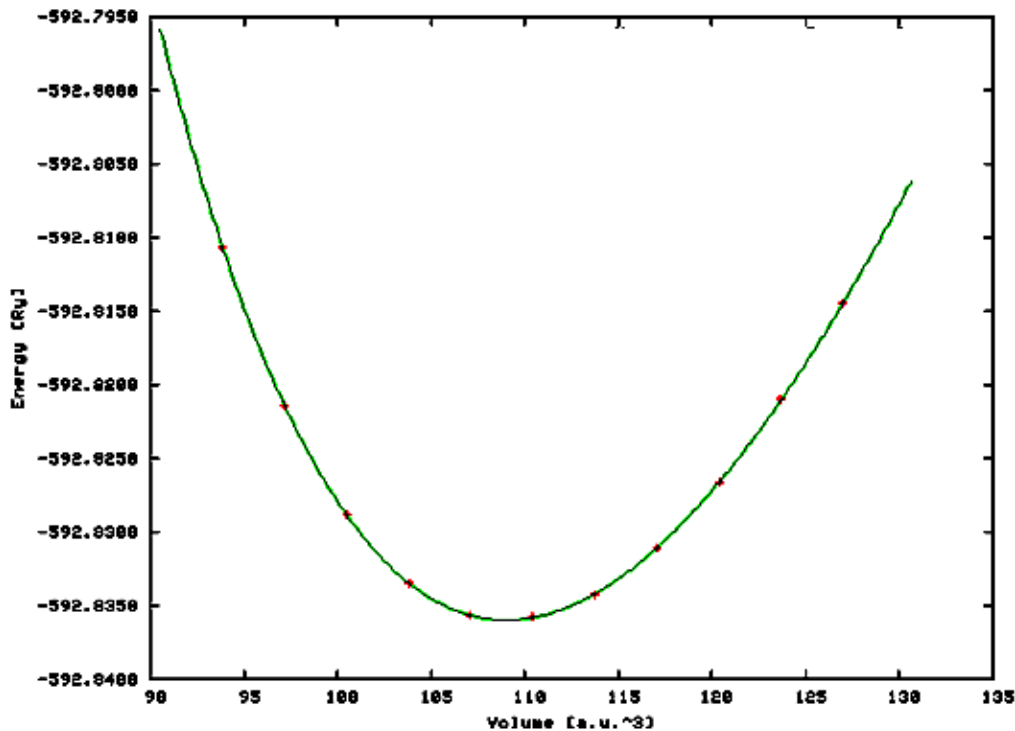


**Figure (4.5): Energy versus volume for RS-AlN using LDA method.**

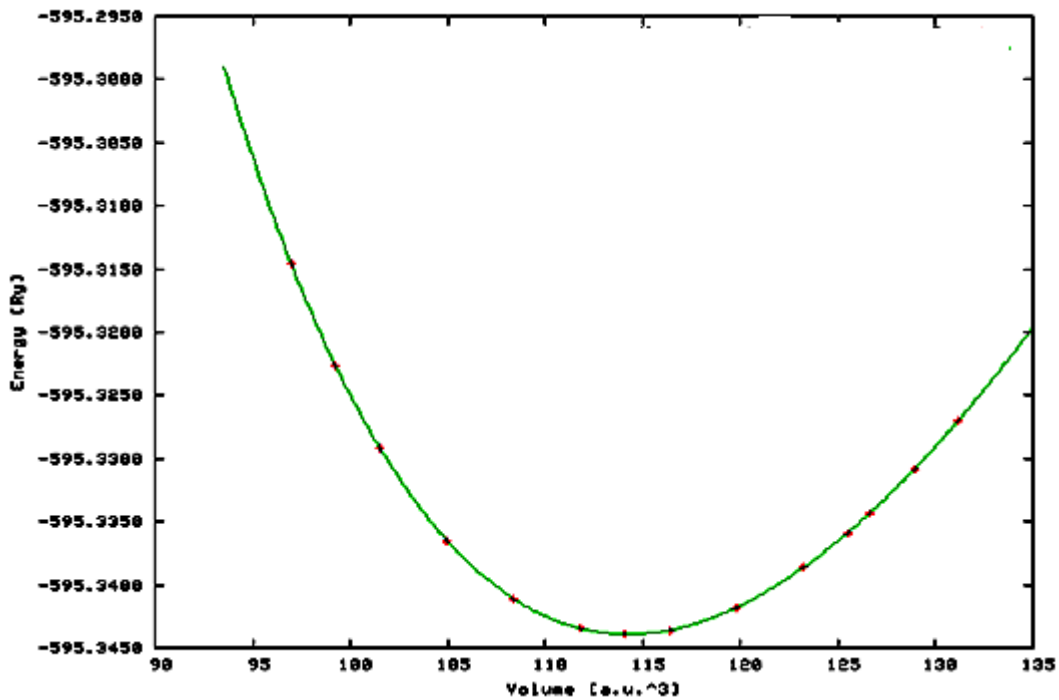


Figure (4.6): Energy versus volume for RS-AlN using GGA method.

Figure 4.5 shows the fitted total energy versus volume for RS-AlN using GGA method, while Figure 4.6 shows the fitted total energy versus volume for RS-AlN using LDA method. The theoretical lattice parameters, bulk modulus and the derivative of bulk modulus to the pressure are obtained through fitting the total energy versus volume data with the Murnaghan's equation of state [74].

### 4.1.2 Band Structure

An energy range in a solid where no electron states exist is called energy band gap. The band gap generally refers to the energy difference between the top of the valence band and the bottom of the conduction band in insulators and semiconductors ; it is the amount of energy required to free an outer shell electron from its orbit about the nucleus to a free state. The semiconductors have a small band gap  $< 3$  eV, also electrons are

confined to a number of bands of energy, and forbidden from other regions[86]. The band gap energy of semiconductors tends to decrease with increasing temperature. When temperature increases, the amplitude of atomic vibrations increase, leading to larger interatomic spacing. The interaction between the lattice phonons and the free electrons and holes will also affect the band gap to a smaller extent [87]. The relationship between band gap energy and temperature can be described by Varshni's empirical expression [88].

$$E_g(T) = E_g(0) - \frac{\alpha T^2}{T + \beta} \quad (4-3)$$

where  $E_g(0)$ ,  $\alpha$  and  $\beta$  are material constants.

Band gaps also depend on pressure. Band gaps can be either direct or indirect band gaps, depending on the band structure.

#### 4.1.2.a Band structure for AlN compound

**Table (4.6): The energy band structures for AlN compound in WZ, RS, and ZB structures.**

Structure	Method	Present calculations(eV)	Other calculations(eV)	Experimental Result (eV)
Wurtzite	LDA	4.425	4.39 <sup>h</sup>	6.28 <sup>k</sup>
	GGA	4.179	4.027 <sup>h</sup>	
Rocksalt	LDA	4.032		
	GGA	4.341		
Zincblende	LDA	2.70	3.21 <sup>h</sup>	
	GGA	3.275	3.304 <sup>h</sup>	

<sup>h</sup> Ref.[1], <sup>k</sup>Ref. [89]

The most features of the band structure of WZ-AlN, RS-AlN and ZB-AlN are shown in Figures 4.7, 4.8 and 4.9 in GGA and LDA methods respectively.

In WZ-AlN the band gap is 4.4 eV, 4.17 eV using LDA and GGA methods respectively, and a direct band gap at  $\Gamma$  point ; this is in agreement with the results of Wright and Nelson [80], who used plane-wave pseudopotential total energy calculation in the LDA approach.

Slight differences are seen in valence bands : In this case GGA bands lie higher in energy than those of LDA which leads to slightly reduction bandwidths.

We notice that the ZB-AlN is indirect band gap from the  $\Gamma$  point, at the X point. Comparing LDA and GGA calculations in the ZB-AlN we see that the band structures are similar, except that the band gap at  $\Gamma$  point for the LDA is smaller than the GGA results.

There is no other calculations about RS-AlN using LDA or GGA methods.

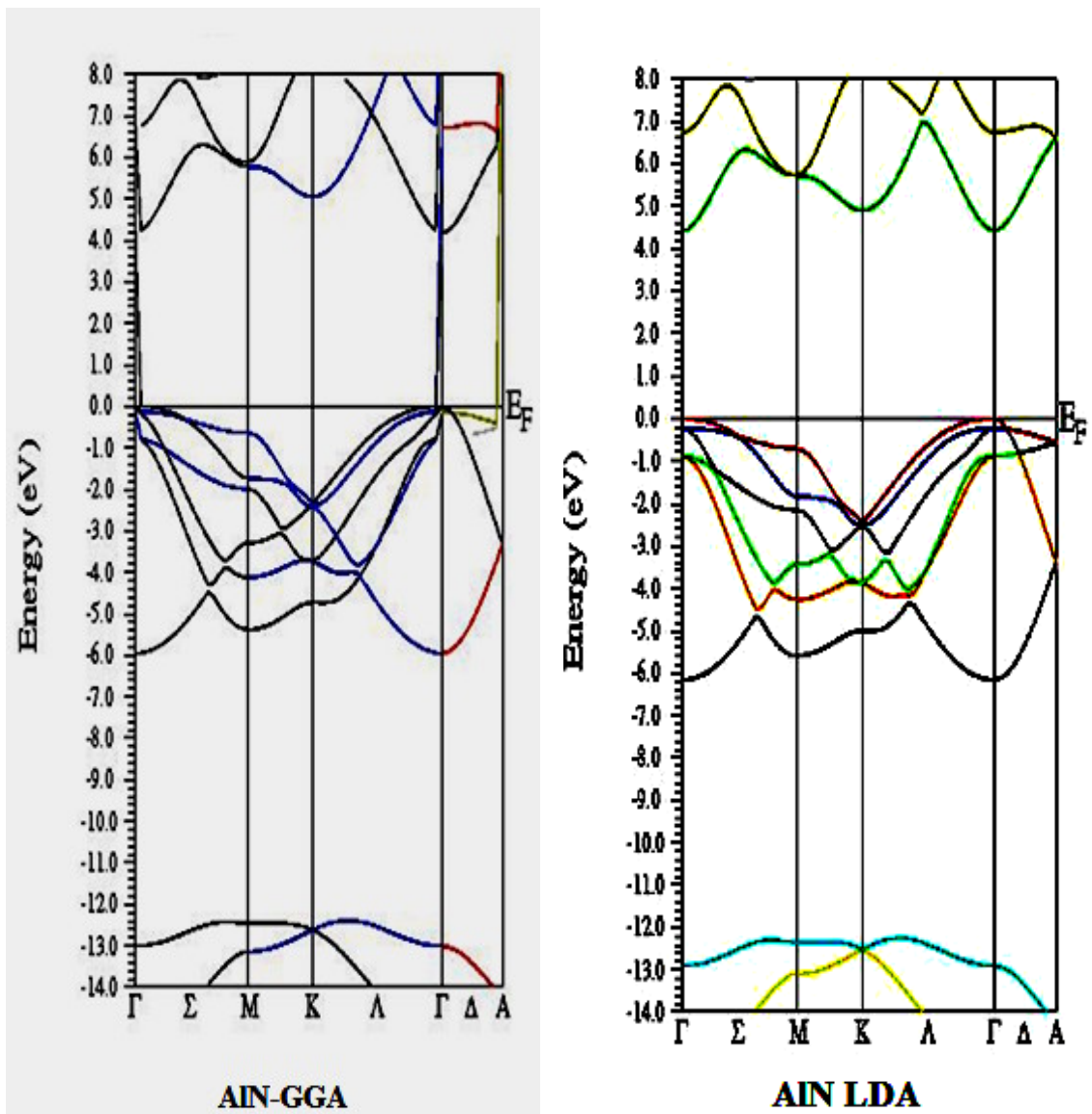


Figure (4.7) : The energy band structure for wurtzite AlN using GGA and LDA methods.

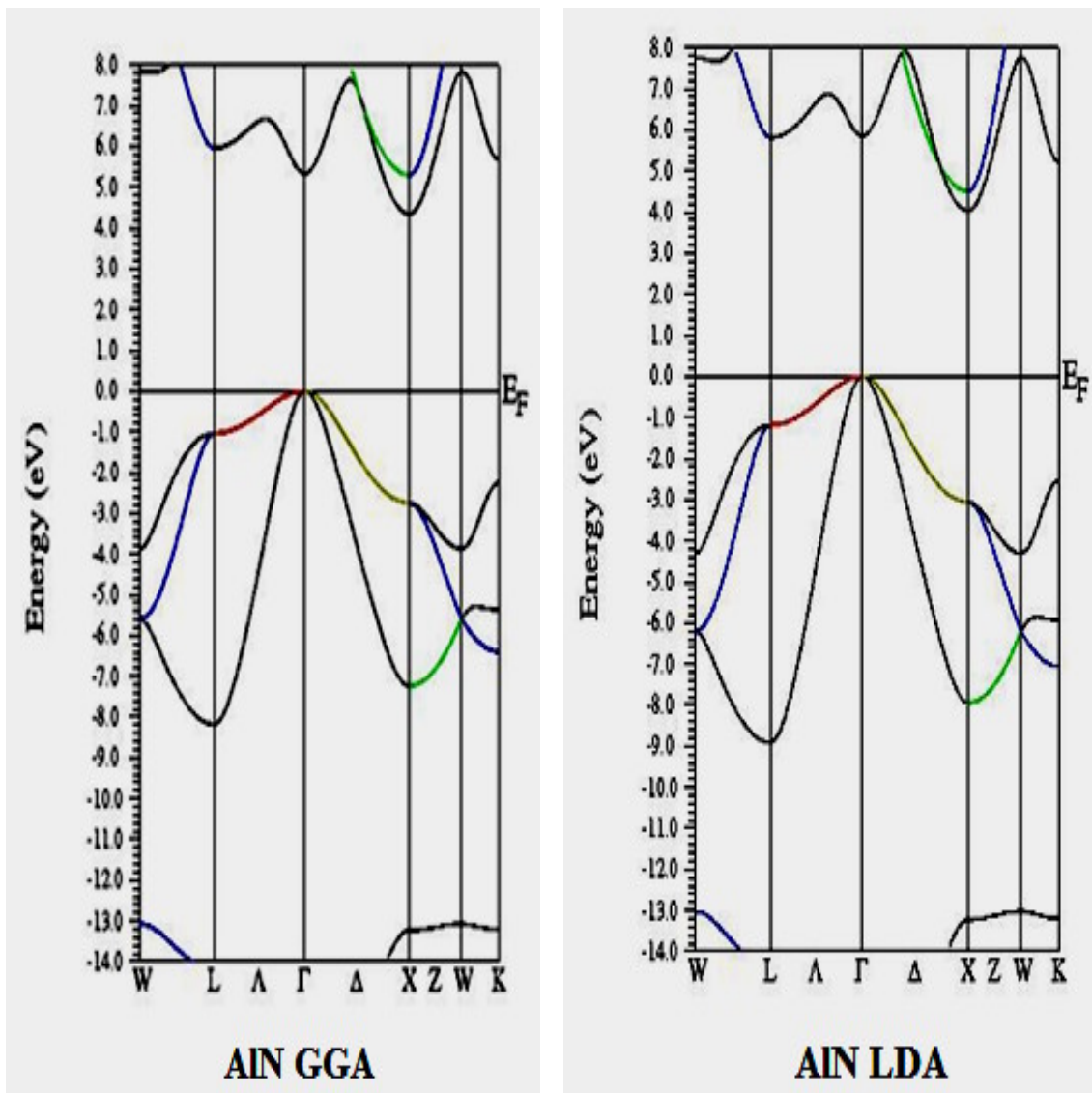
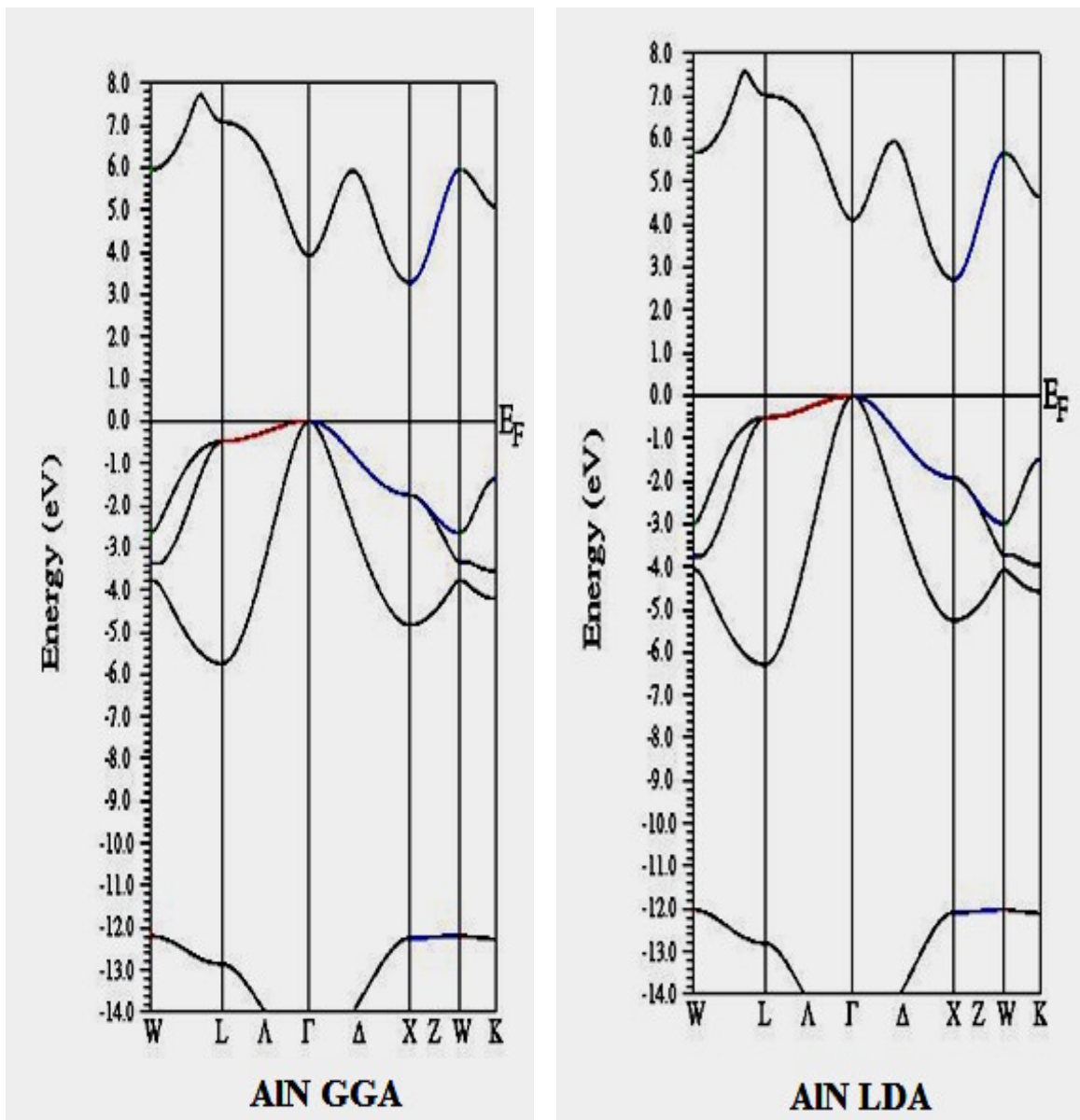


Figure (4.8) : The energy band structure for rocksalt AlN using GGA and LDA methods.



**Figure (4.9):** The energy band structure for zincblende AlN using GGA and LDA methods.

#### 4.1.3 Structural phase transition:

When a system of molecules undergoes change, whether chemical reaction or changes in physical states such as phase changes. There are two tendencies driving the changes:

- Free Energy tends to decrease,
- Entropy tends to increase.

If  $E$  represents the energy,  $T$  the temperature, and  $S$  the entropy, these two tendencies can be combined by stating that the expression  $E - TS$ , the Helmholtz function, tends to decrease. Strictly, this is only true in situations where the volume is constant, as in sealed containers. If the pressure is constant, as in open containers, the enthalpy  $H = E + PV$  (where  $P$  represents the pressure and  $V$  represents the volume) replaces the energy, and thus the quantity that must be minimized is  $H - TS = E + PV - TS$ , the Gibbs function. When  $T=0$ , then  $H= E +PV$  and then we can get the pressure.

Physicists have tended to use the term free energy and the symbol  $F$  for the Helmholtz function, using  $G$  to represent the Gibbs function; chemists have preferred to denote the Helmholtz function by  $A$  and call it the work content, reserving the term free energy and the symbol  $F$  for the Gibbs function. Recently a compromise notation has become common, using  $A$  for the Helmholtz function,  $G$  for the Gibbs function, and avoiding  $F$  entirely. The functions are then referred to as the Helmholtz free energy and Gibbs free energy[90].

**Table (4.7): Transition pressure ( $P_t$ ) of AlN structure using LDA and GGA methods.**

Structure	Method	$P_t$ (GPa)		
		Present	Other	Experimental Results
ZB-RS	GGA	4.64	5.3 <sup>h</sup>	
WZ-RS	GGA	10	9.5 <sup>h</sup>	14 <sup>i</sup> , 16 <sup>j</sup>
ZB-RS	LDA	3	7 <sup>a</sup>	
WZ-RS	LDA	9.3	12.9 <sup>l</sup> , 16.6 <sup>h</sup>	

<sup>h</sup>Ref.[1], <sup>i</sup>Ref. [84], <sup>j</sup>Ref.[85], <sup>l</sup>Ref.[91],

Figures 4.10 and 4.11 show the fitted energy versus volume for AlN. The transition pressure  $p_t$  from WZ to RS and ZB to RS of AlN is determined. The  $p_t$  for WZ to RS is found to be 10 GPa and for ZB to RS is found to be 4.64 GPa within GGA calculations. Whereas the ( $p_t$ ) from WZ to RS and ZB to RS of AlN is found to be 9.3 GPa, 3GPa respectively, within LDA calculations. From the Figures we notice that the WZ structure is the stable structure for AlN.

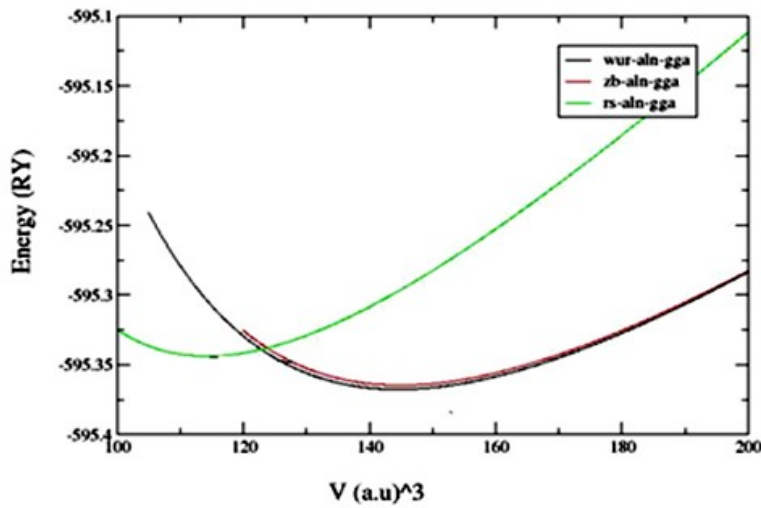


Figure (4.10): The transition pressure of AlN using GGA method.

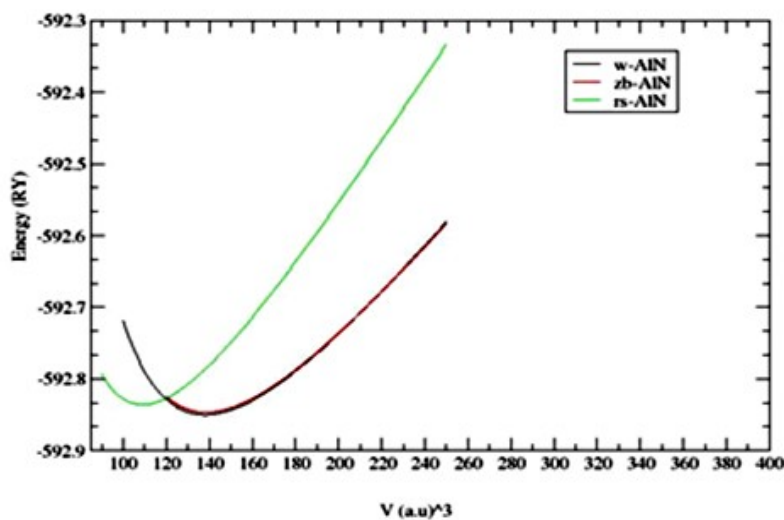


Figure (4.11): The transition pressure of AlN using LDA method.

## 4.2 BN Compound:

Boron nitride possesses many properties which are of technological interest. It is used as an electrical insulator however its tendency to oxidise at high temperatures often restrict its use to vacuum and inert atmosphere operation. Also, its chemical inertness leads to application as thermocouple protection sheaths, crucibles and linings for reaction vessels though as above oxidation must be avoided. In its dense cubic zincblende form, boron nitride has extreme hardness, high melting point, wide band gap, chemical inertness, and large thermal conductivity.

### 4.2.1 Structural properties:

**Table (4.8): The structural parameters for zincblende-BN structure using LDA and GGA methods**

Method	a ( )		B (GPa)		B' (GPa)	
	Present	Other	Present	Other	Present	Other
LDA	3.595	3.575 <sup>n</sup>	403.7575	397 <sup>n</sup> , 386 <sup>n</sup>	4.1791	3.97 <sup>n</sup> , 4 <sup>n</sup>
GGA	3.626 <sup>p</sup>	3.623 <sup>n</sup> , 3.606 <sup>n</sup>	370.9779	368 <sup>n</sup> , 360 <sup>n</sup>	3.5891	3.3 <sup>n</sup> , 4 <sup>n</sup> , 3.6 <sup>n</sup>
<b>Experimental Results</b>	3.615 <sup>m</sup>		369 <sup>m</sup>		4 <sup>m</sup>	

<sup>m</sup>Ref.[92], <sup>n</sup>Ref.[93]

The curves of Figures 4.12, 4.13 are fitted to Murnaghan's equation of state in order to determine the structural parameters given in tables 4.8 and 4.9. In table 4.8, the lattice constant in GGA method is in a good agreement with the experimental value whereas it is found that the LDA calculation is slightly lower than the experimental value. In addition, the

Bulk modulus value is closed to the experimental value in GGA method but in LDA is slightly larger. In the LDA, the  $B'$  is in good agreement with the experimental value.

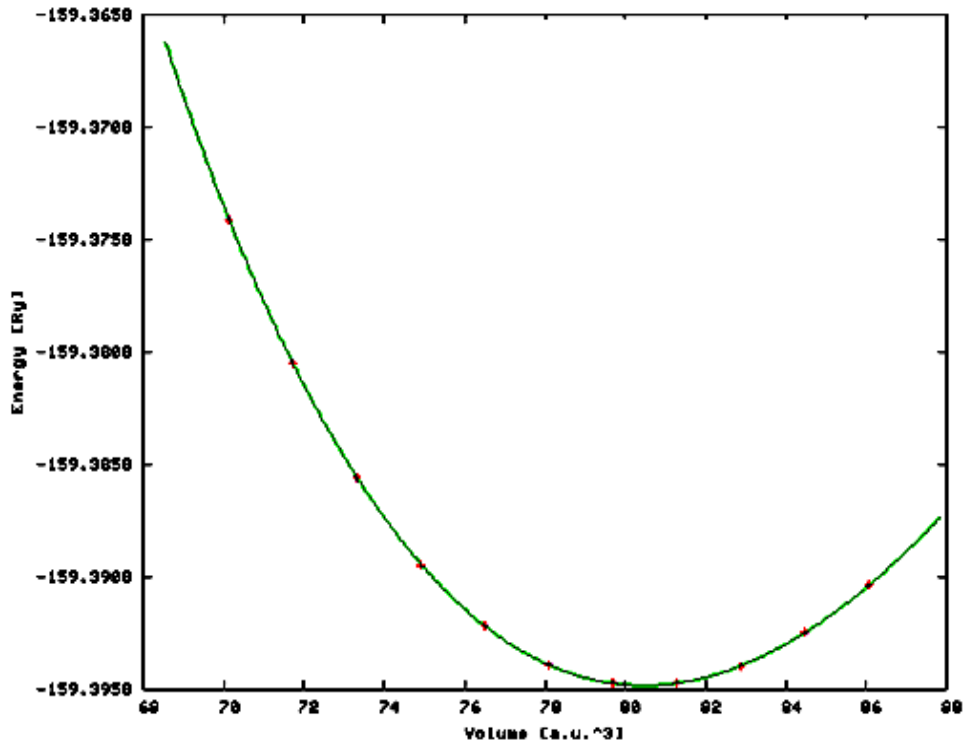


Figure (4.12): Energy versus volume for ZB-BN using GGA method.

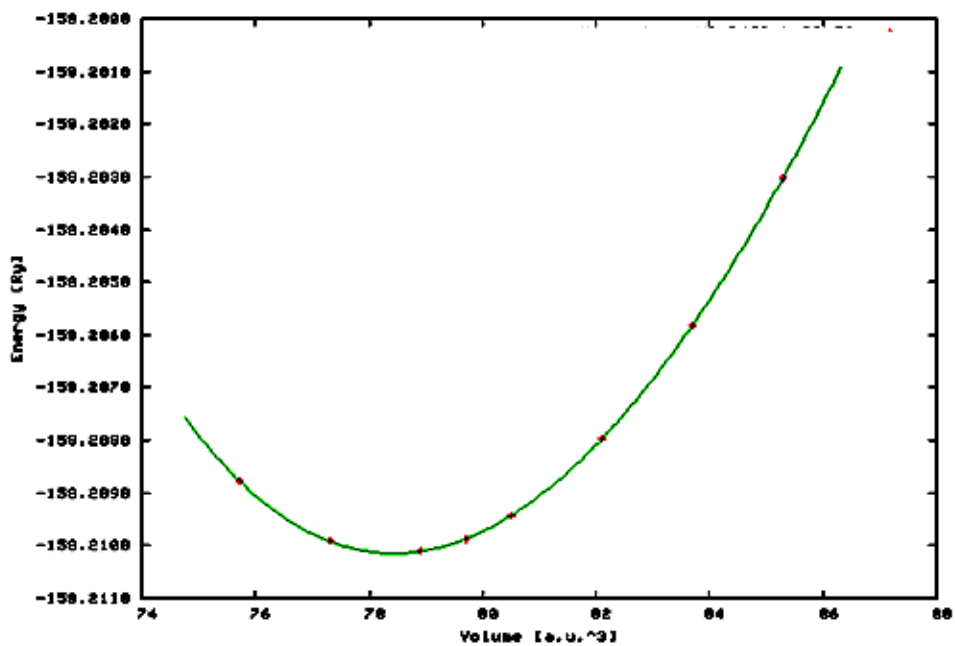


Figure (4.13): Energy versus volume for ZB-BN using LDA method

**Table (4.9): The structural parameters for rocksalt-BN structure using LDA and GGA methods.**

Method	a ( )		B (GPa)		B' (GPa)	
	Present	Other	Present	Other	Present	Other
LDA	3.467	3.500 <sup>n</sup> 3.493 <sup>n</sup>	428.6748	425 <sup>n</sup>	4.2683	4.59 <sup>n</sup>
GGA	3.5041	3.503 <sup>n</sup> , 3.49 <sup>n</sup>	381.4622	399 <sup>n</sup> , 480 <sup>n</sup>	3.7236	2.53 <sup>n</sup> , 3.7 <sup>n</sup>

<sup>n</sup>Ref.[93]

Table 4.9 shows the structural parameters (a, B, B') compared with other calculations.

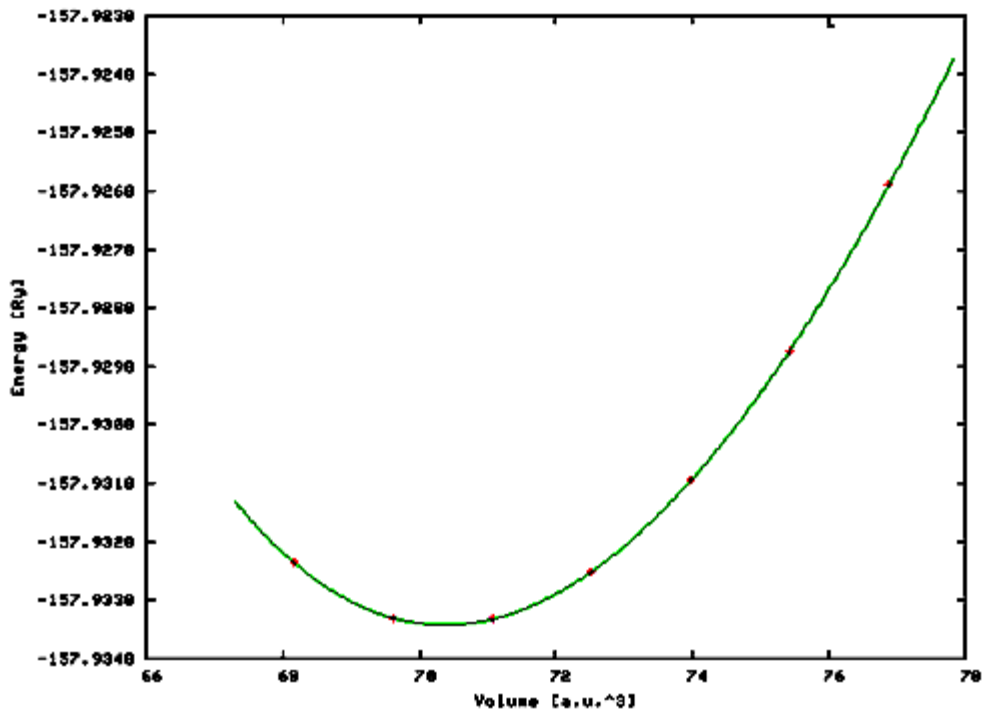


**Figure (4.14): Energy versus volume for RS-BN using LDA method**

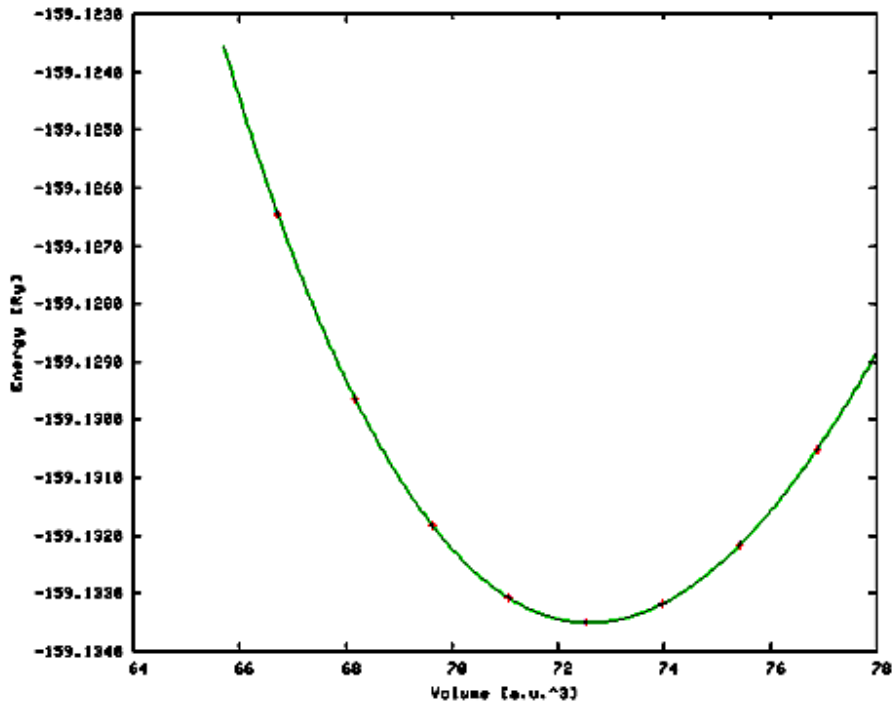


Figure (4.15): Energy versus volume for RS-BN using GGA method

Figures 4.14 and 4.15 show the fitted energy versus volume for RS-BN using LDA and GGA method which the structural properties are obtained from them.

#### 4.2.2 Band structure

Table (4.10): The energy band structure for BN compound

Structure	Method	Present calculations (eV)	Other calculations (eV)	Experimental Result (eV)
Zincblende	LDA	4.356	4.2 <sup>n</sup> , 4.4 <sup>n</sup>	6 <sup>n</sup>
	GGA	4.433		6.4 <sup>n</sup>
Rocksalt	LDA	2.193	6.3 <sup>n</sup>	6.4 <sup>n</sup>
	GGA	1.710		

<sup>n</sup>Ref.[93]

Figures 4.16, 4.17 show the energy band gap for ZB-BN and RS-BN, which present that these band structures are calculated at the equilibrium lattice constants for the LDA and GGA methods. It is found to be 4.35 eV

and 4.43 eV, 2.19 eV and 1.71eV by LDA and GGA respectively. We notice that the energy band gap for ZB-BN is indirect ( $\Gamma$ -X). The energy band gap for ZB -BN in GGA method is in close agreement with other calculations. Also, the energy band gap for RS-BN is indirect (L-X).

The conduction bands in LDA calculations are shifted a little down with respect to those of the GGA which is leading to a reduction of the band within the ZB-BN structure. This is in contrast in RS-BN structure.

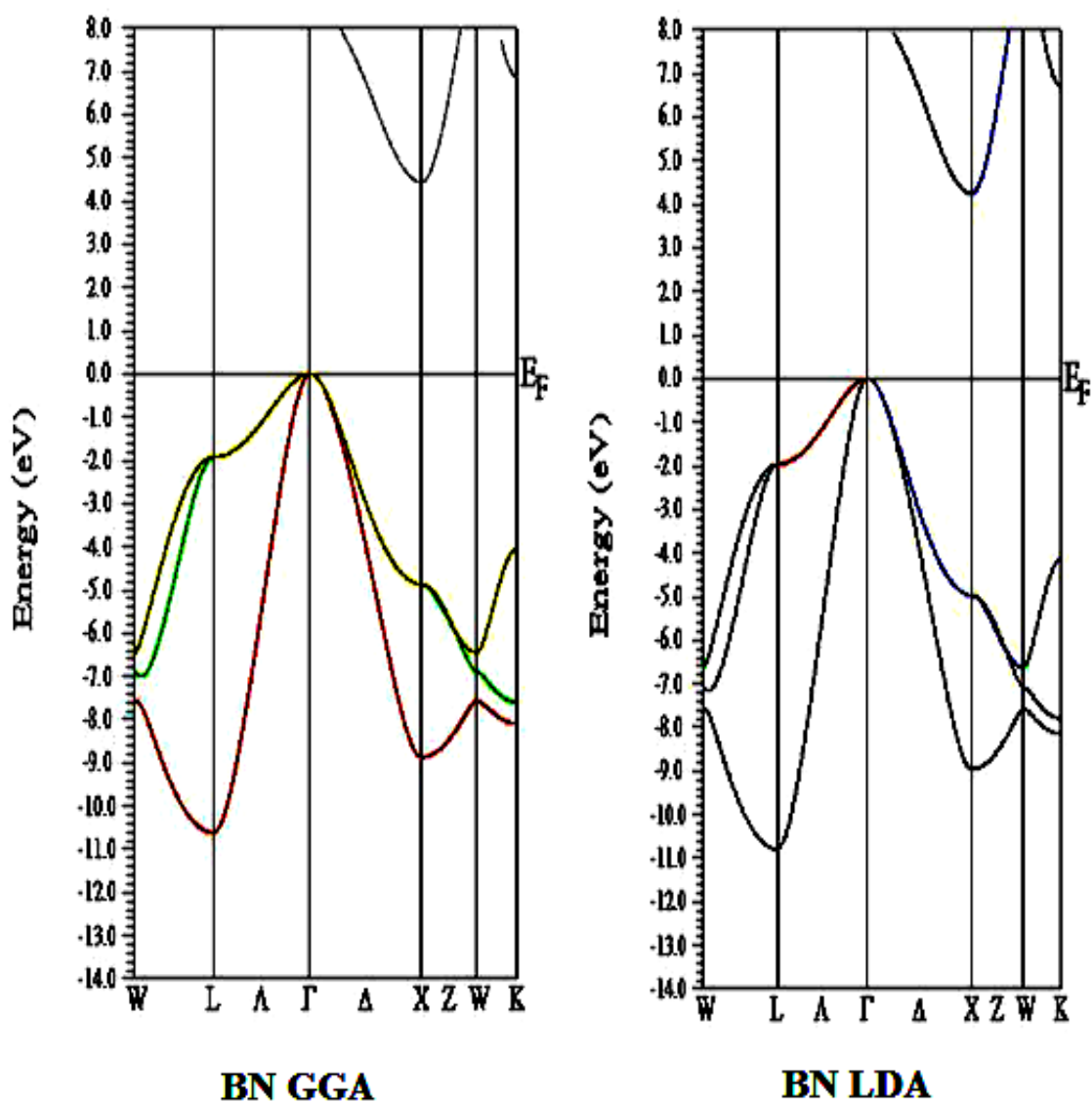


Figure (4.16): The energy band structure for zincblende BN using GGA and LDA methods.

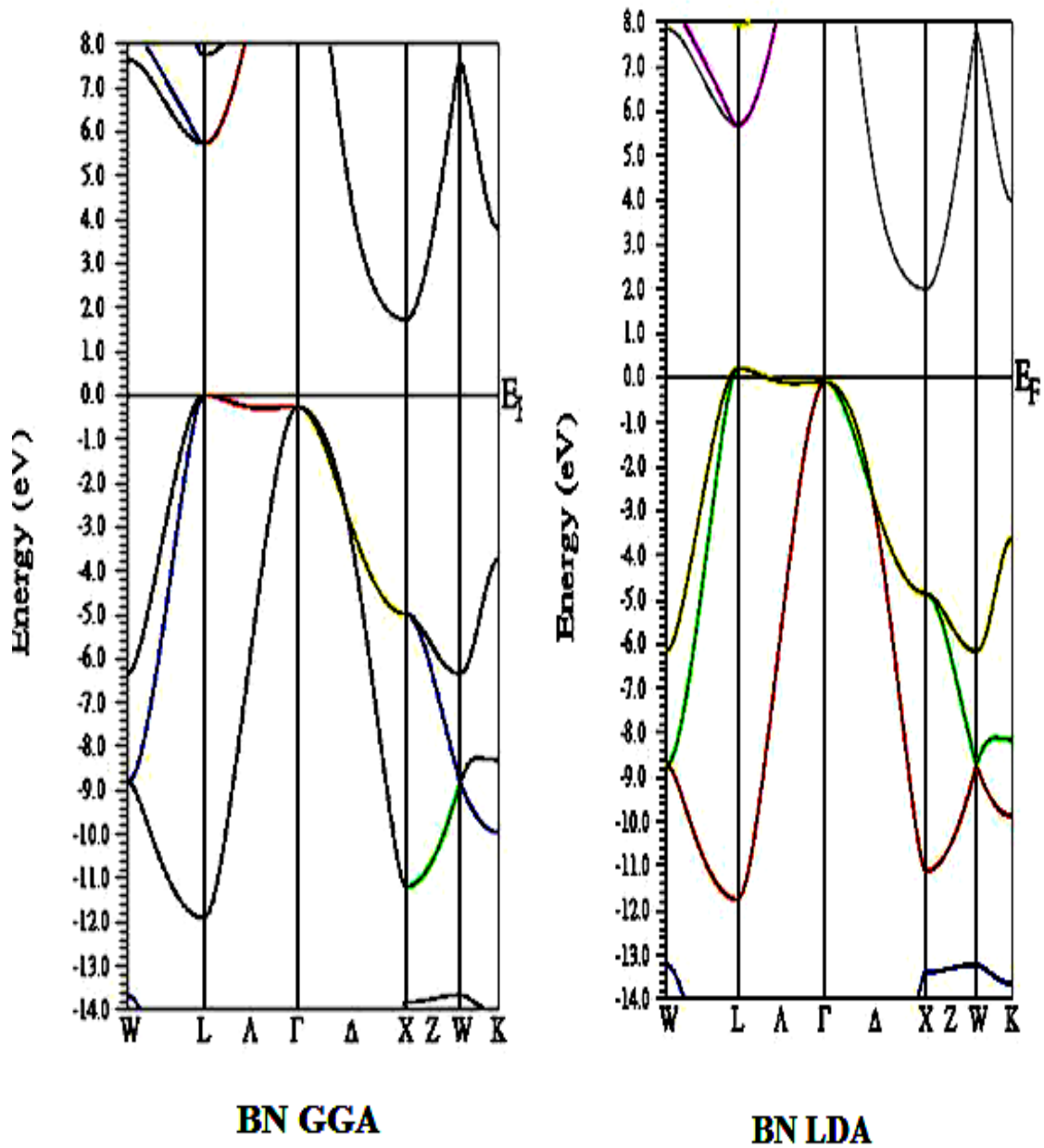


Figure (4.17): The energy band structure for rocksalt BN using GGA and LDA methods

#### 4.2.3 Structural phase transition:

Table (4.11): Transition pressure ( $P_t$ ) of BN structure using GGA method

Structure	Method	$P_t$ (GPa)	
		Present	Other(GPa)
ZB-RS	GGA	500	555 <sup>n</sup> , 111 <sup>n</sup>

<sup>n</sup>Ref.[93]

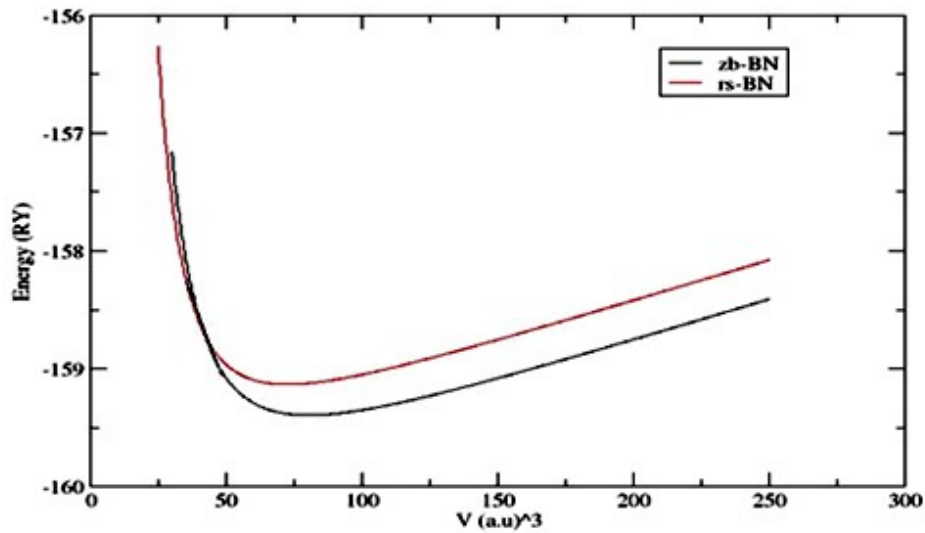


**Figure (4.18): The transition pressure of BN using GGA method**

Figure 4.18 shows that the  $P_t$  for ZB to RS in BN is 500 GPa. This result is in a good agreement with other calculations. From the Figure we notice that the ZB structure is the stable structure for BN.

### **4.3 InN compound:**

#### **4.3.1 Structural properties:**

Recently, InN has attracted considerable attention due to its potential applications, on one side, and the seemingly conflicting results of various investigations, on the other side.

**Table (4.12):The structural parameters for Wurtzite-InN structure using LDA and GGA methods.**

Method		LDA	GGA	Experimental Results
a ( )	Present	3.514	3.594	3.54 <sup>P</sup>
	Other	3.52 <sup>o</sup>	3.58 <sup>o</sup>	
c ( )	Present	5.692	5.786	
	Other	5.702 <sup>o</sup>	5.763 <sup>o</sup>	
c/a	Present	1.62	1.61	1.611 <sup>o</sup>
	Other	1.62 <sup>o</sup>	1.61 <sup>o</sup>	
u	Present	0.375	0.379	0.375 <sup>o</sup>
	Other	0.3788 <sup>o</sup>	0.379 <sup>o</sup>	
B (GPa)	Present	149.0221	122.7514	125.5 <sup>o</sup>
	Other	142.58 <sup>o</sup>	123.51 <sup>o</sup>	
B' (GPa)	Present	4.7825	5.2645	12.7 <sup>o</sup>
	Other	4.67 <sup>o</sup>	4.43 <sup>o</sup>	

<sup>o</sup>Ref. [94]. <sup>P</sup>Ref.[95]

In our GGA calculation seem to be accurate when compared with the experimental value. Moreover, the u parameter in LDA calculation is accurate compared to the experimental value. The Bulk modulus (B) obtained using LDA is larger than experimental value, whereas the B is smaller using GGA method.

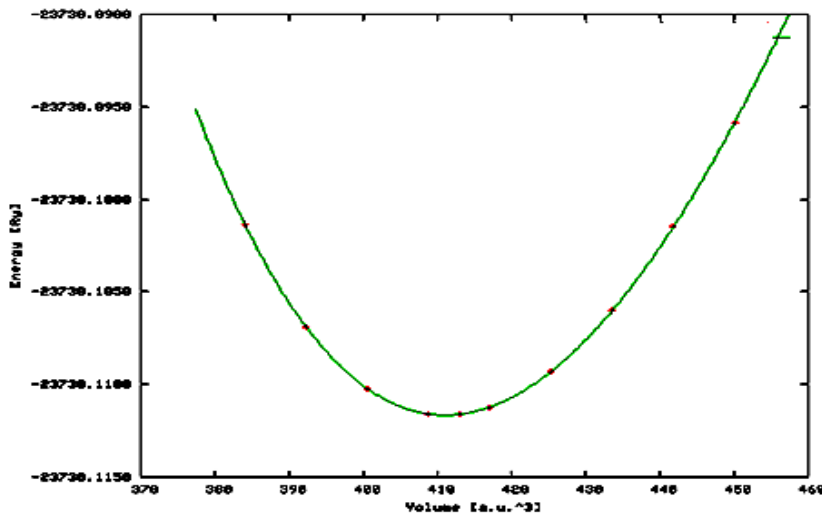


**Figure (4.19): Energy versus volume for WZ-InN using LDA method**

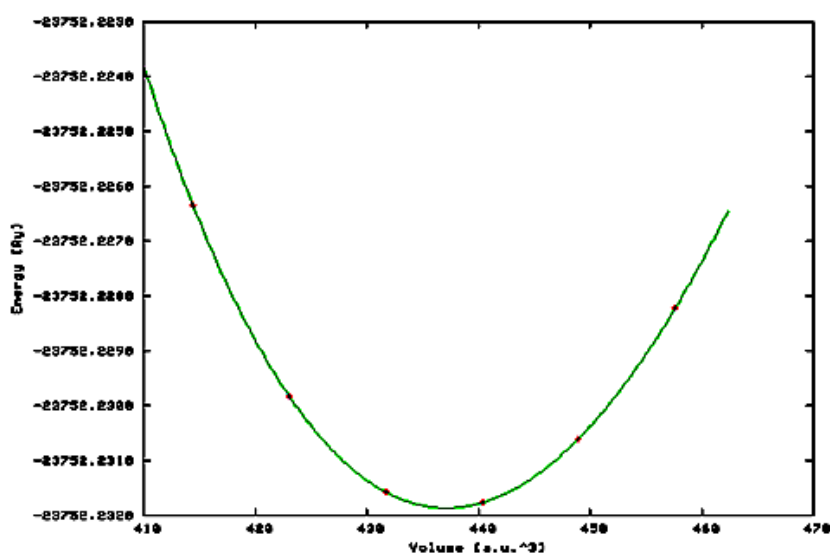


Figure (4.20): Energy versus volume for WZ-InN using GGA method

Figures 4.19 and 4.20 show the fitted energy versus volume for WZ-InN using LDA and GGA method which the structural properties are obtained from them.

**Table (4.13): The structural parameters for Rocksalt-InN structure using LDA and GGA methods.**

Method	a ( )		B(GPa)		B' (GPa)	
	Present	Other	Present	Other	Present	Other
LDA	4.603	4.63 <sup>o</sup>	196.2893	186.2 <sup>o</sup>	6.2854	4.67 <sup>o</sup>
GGA	4.709	4.71 <sup>o</sup>	151.1941	161.45 <sup>o</sup>	3.5766	4.45 <sup>o</sup>
<b>Experimental Results</b>			170 <sup>g</sup>		5.09 <sup>g</sup>	

<sup>o</sup>Ref.[94]. <sup>g</sup>Ref.[83]

As shown in table 4.13, the lattice constant is close to other calculations. The bulk modulus (B) in LDA is larger than experimental value but GGA calculations show that B is smaller than the experimental values. We notice that B` in both LDA and GGA appears to be in reasonable agreement with experimental value. Figures 4.21 and 4.22 show

the fitted energy versus volume for RS-InN using LDA and GGA methods.

The structural properties ( $a$ ,  $B$ , and  $B'$ ) are obtained from them.

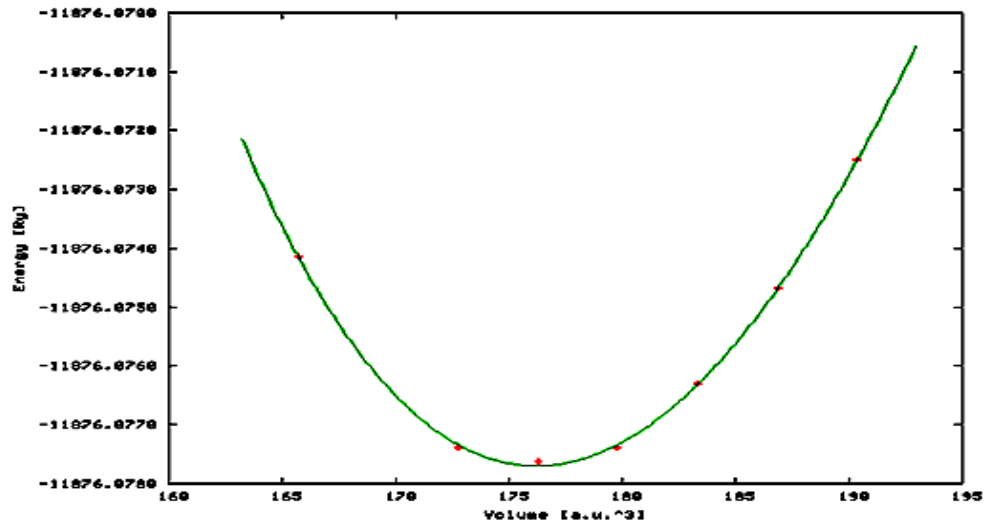


Figure (4.21): Energy versus volume for RS-InN using GGA method

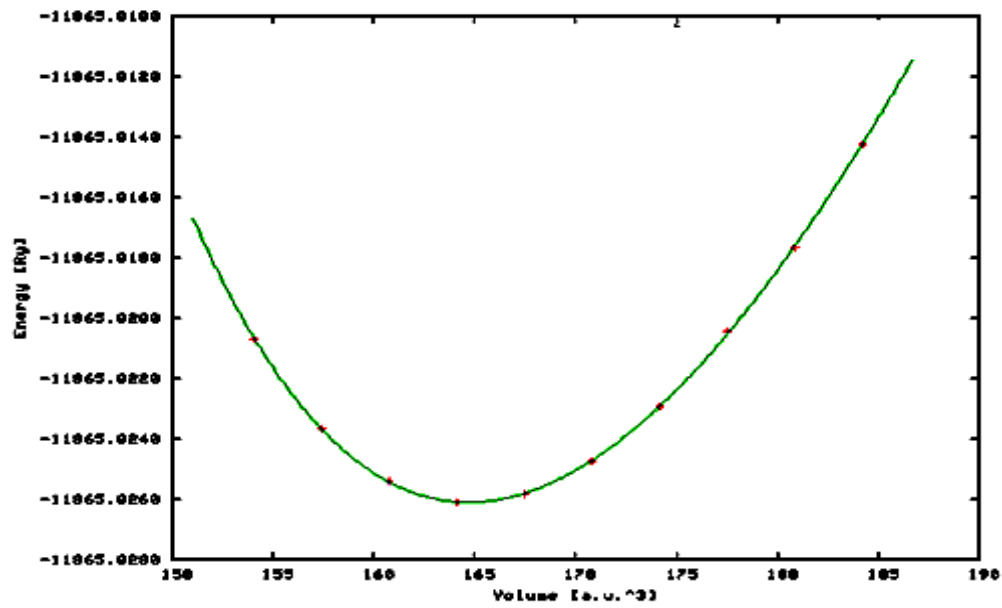


Figure (4.22): Energy versus volume for RS-InN using LDA method

**Table (4.14): The structural parameters for ZB-InN structure using LDA and GGA methods.**

Method	a ( )		B (GPa)		B' (GPa)	
	Present	Other	Present	Other	Present	Other
LDA	4.94	4.96 <sup>o</sup>	148.5.94	142.37 <sup>o</sup>	4.8702	4.69 <sup>o</sup>
GGA	5.06	5.04 <sup>o</sup>	122.0732	123.23 <sup>o</sup>	4.7914	4.44 <sup>o</sup>
<b>Experimental Results</b>	4.98 <sup>g</sup>		137 <sup>g</sup>			

<sup>o</sup> Ref.[94], <sup>g</sup> Ref.[83]

In table 4.14, the lattice constant of ZB-InN in LDA calculation seems to be in a good agreement compared to the experimental value. In GGA method the value of B is smaller when compared with the LDA and experimental value. The B' in LDA calculation is larger than in GGA calculation.

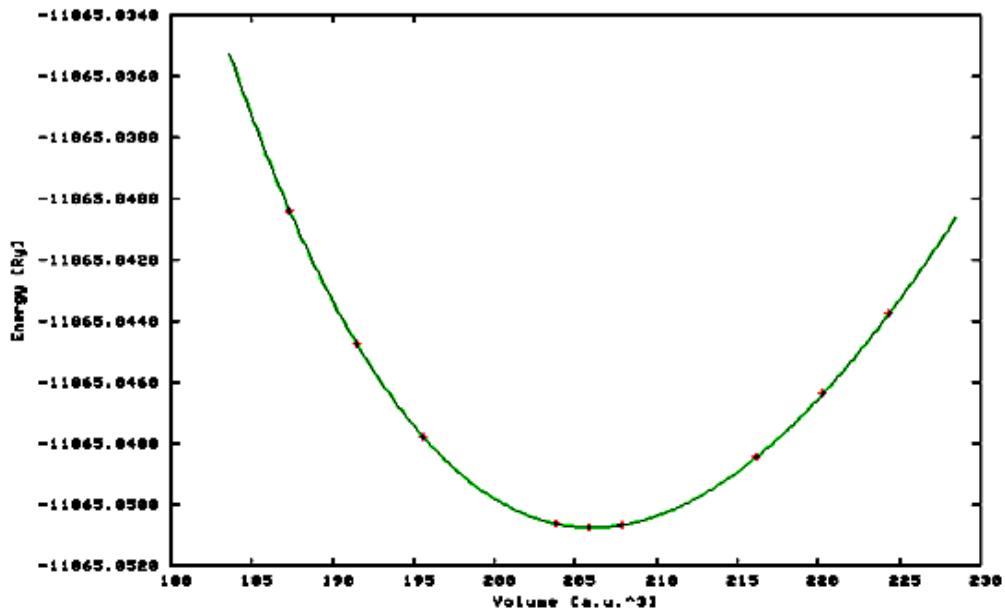


**Figure (4.23): Energy versus volume for ZB-InN using LDA method**

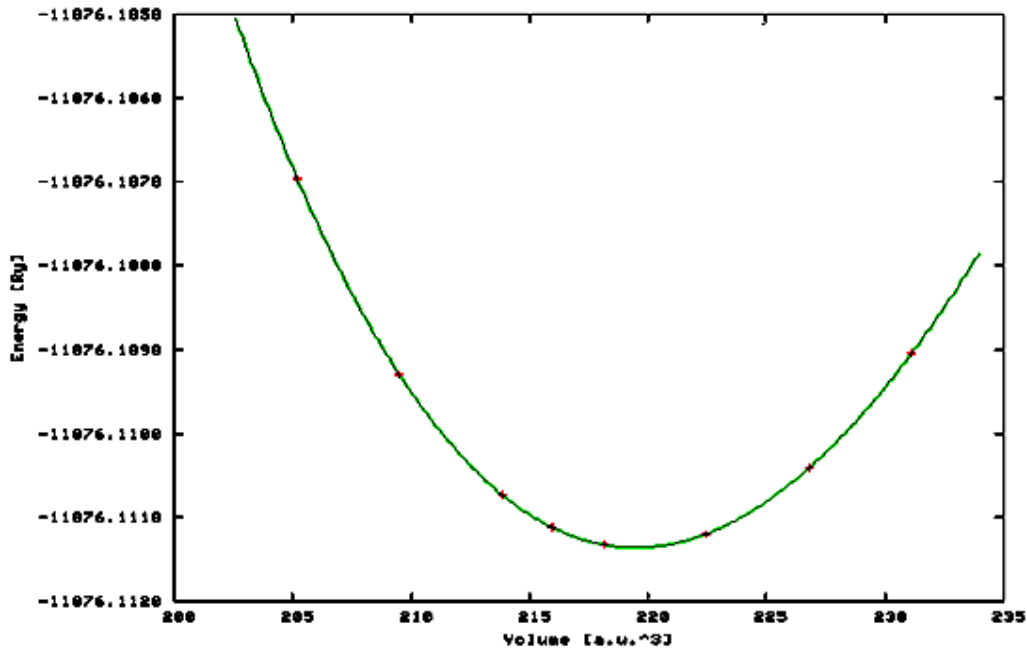


Figure (4.24): Energy versus volume for ZB-InN using GGA method

Figures 4.23 and 4.24 show the fitted energy versus volume for ZB-InN using LDA and GGA method which the structural properties are obtained from them.

### 4.3.2 Band structure

Table (4.15): The energy band structure for InN compound

Structure	Method	Present calculations(eV)	Other calculations(eV)
Wurtzite	LDA	-0.2640	-0.27 <sup>q</sup>
	GGA	-0.3643	-0.37 <sup>q</sup>
Rocksalt	LDA	0.0838	
	GGA	-0.2770	
Zincblende	LDA	-0.38962	-0.2 <sup>q</sup> , -0.4 <sup>q</sup>
	GGA	-0.51361	-0.55 <sup>q</sup>

<sup>q</sup>Ref.[96].

In table 4.15 we notice that the energy band gap for InN compound in all structures is small. The energy band gap for InN compound in LDA

and GGA calculations seem to be in a good agreement compared to the other calculations. The energy band gap for InN compound in LDA calculation is overestimated than the energy band gap in GGA calculation.

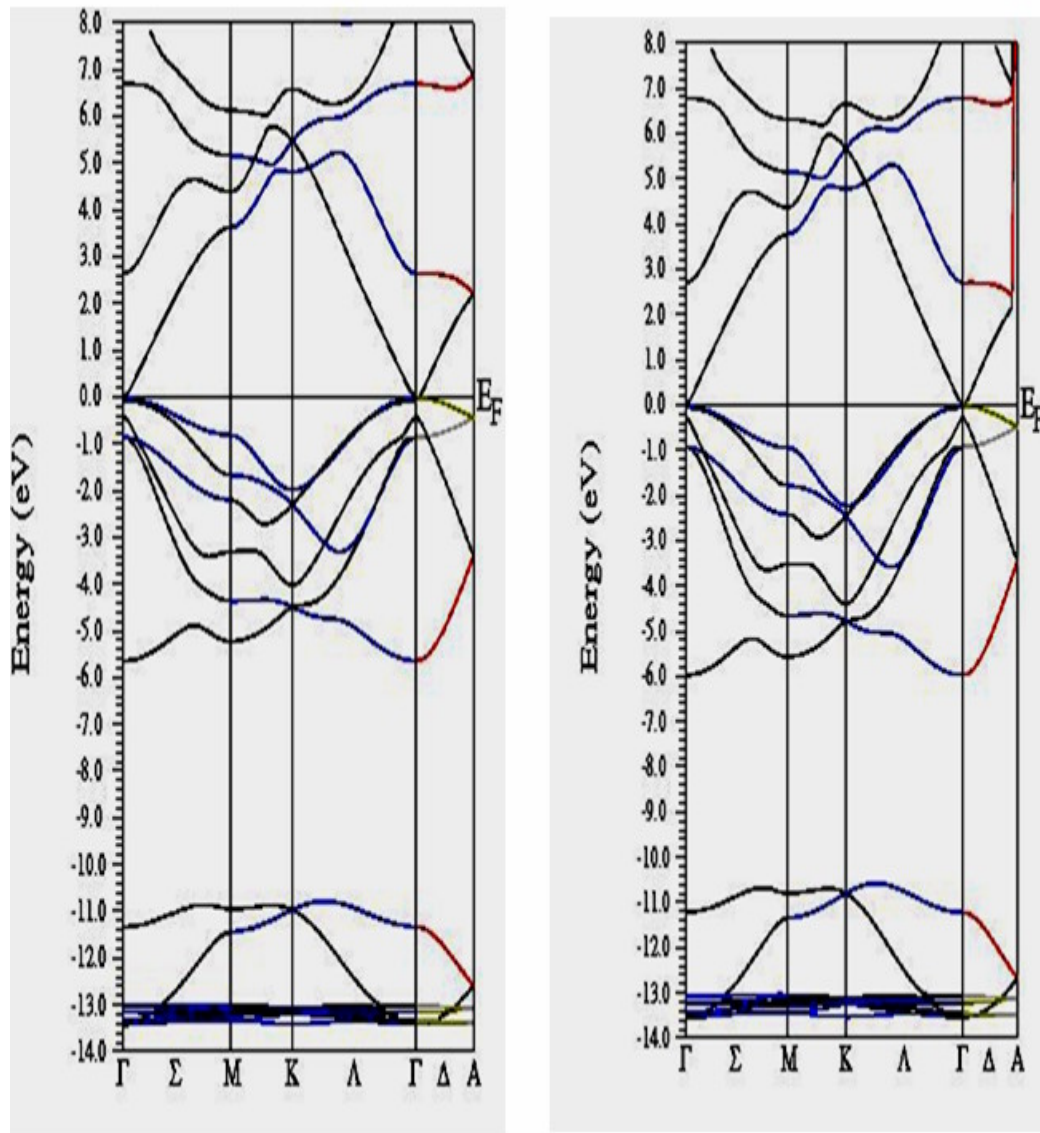


**Figure (4.25):** The energy band structure for wurtzite InN using GGA and LDA methods.

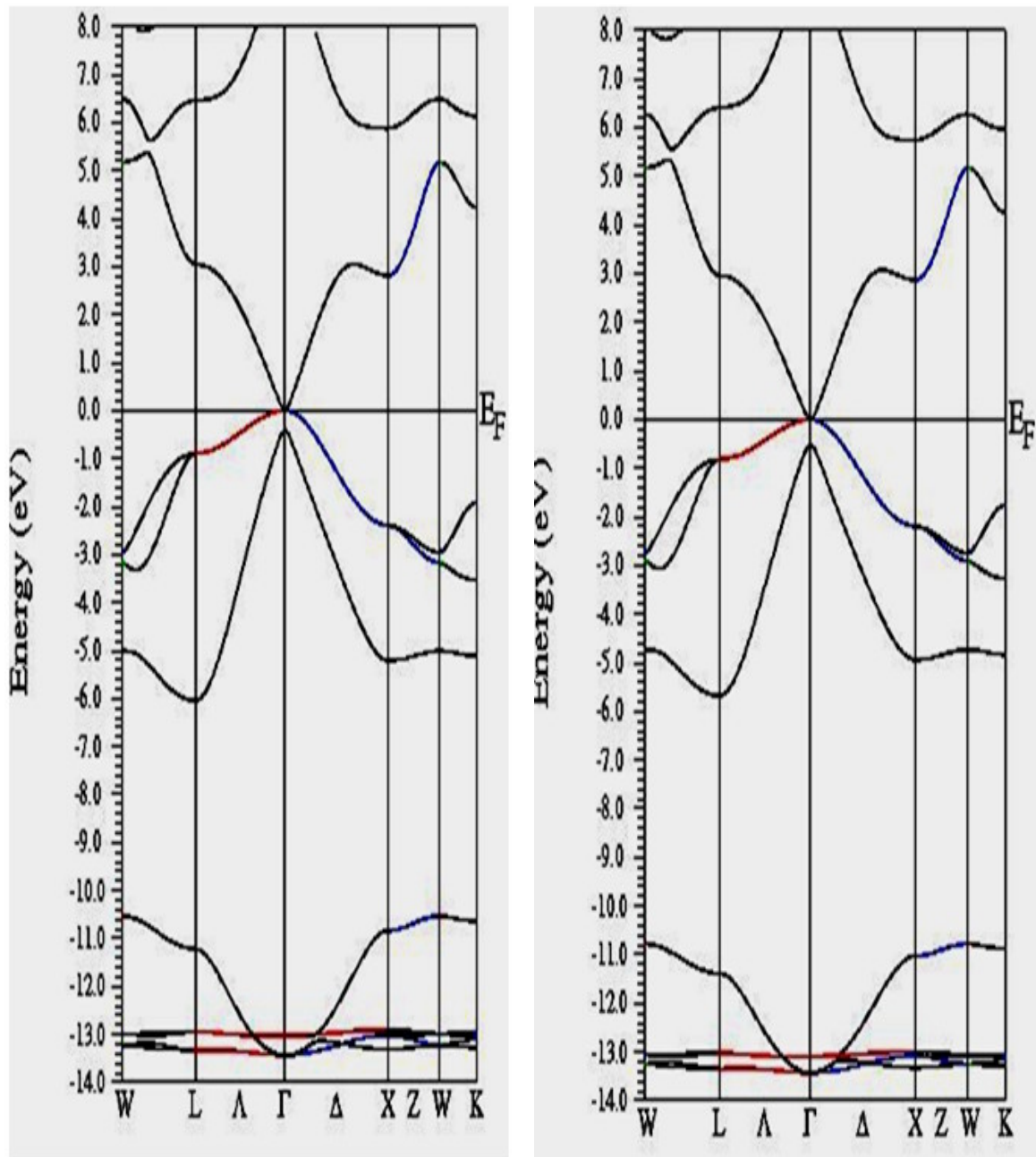


**Figure (4.26):** The energy band structure for zincblende InN using GGA and LDA methods.

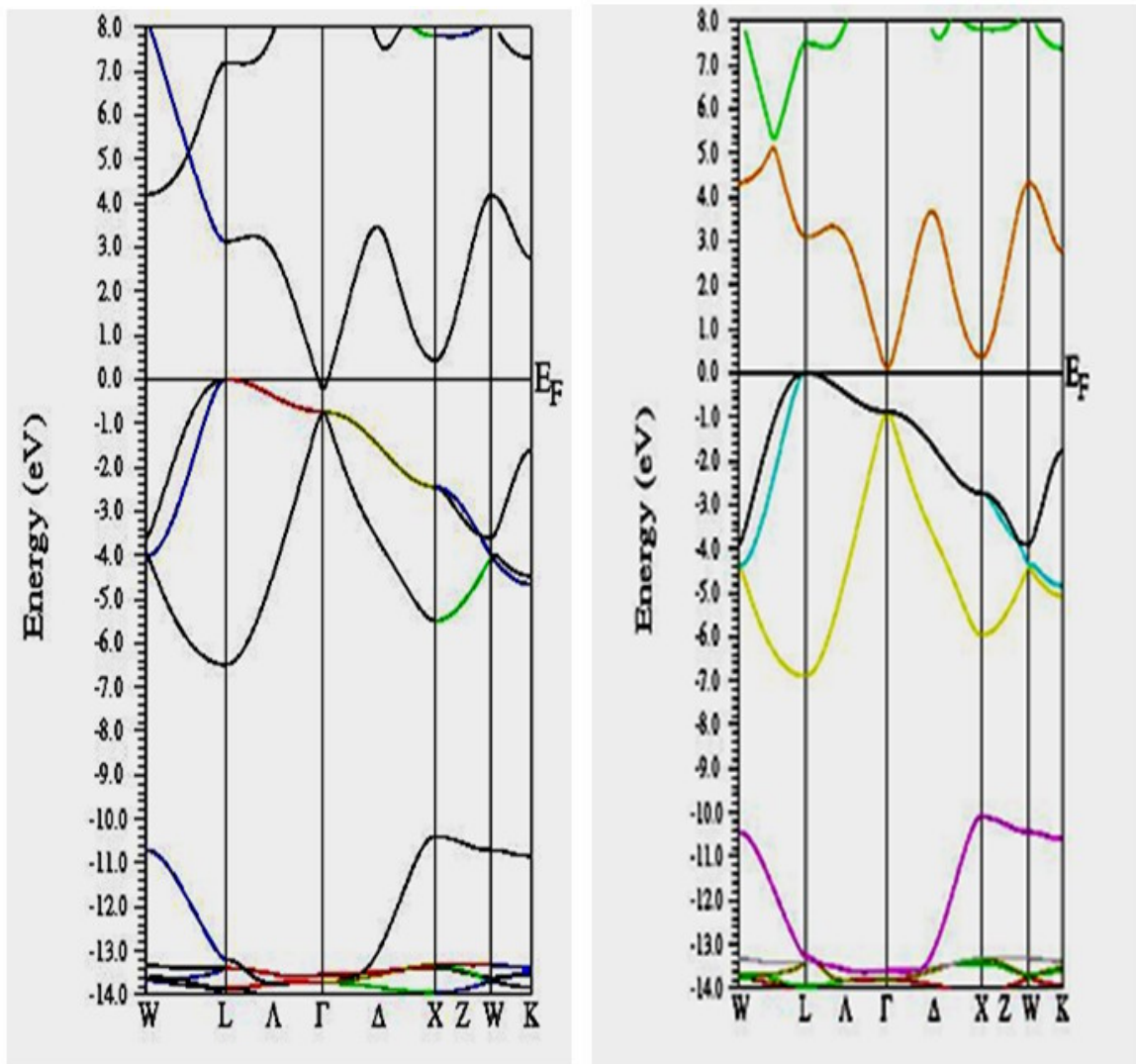


**Figure (4.27):** The energy band structure for rocksalt InN using GGA and LDA methods.

In Figures 4. 25 and 4. 26 the band structure of InN in the ZB and the WZ structures appear quite similar, with no band gap at  $\Gamma$  for LDA and GGA in the ZB and WZ structures.

In WZ-InN the energy band gap is  $-0.264\text{eV}$ ,  $-0.3643\text{eV}$  using LDA and GGA methods respectively, and a direct band gap at  $\Gamma$  point ; this is in agreement with the results of plane-wave pseudopotential total energy calculation in the LDA approach [96].

We notice that the in RS-InN is indirect band gap from the L point, at the  $\Gamma$  point. There is no calculations about RS-InN using LDA or GGA methods.

### 4.3.3 Structural phase transition:

**Table (4.16): Transition pressure ( $P_t$ ) of InN structure using GGA method**

Structure	Method	$P_t$ (GPa)		
		Present	Other	Experimental Results
WZ-RS	GGA	16.6	12.47 <sup>h</sup> , 11 <sup>h</sup>	12.1 <sup>r</sup> , 10 <sup>s</sup>
ZB-RS	GGA	18.5	10 <sup>h</sup> , 21.6 <sup>t</sup>	

<sup>h</sup> Ref.[1], <sup>r</sup>Ref.[97], <sup>s</sup>Ref.[98], <sup>t</sup>Ref.[99].

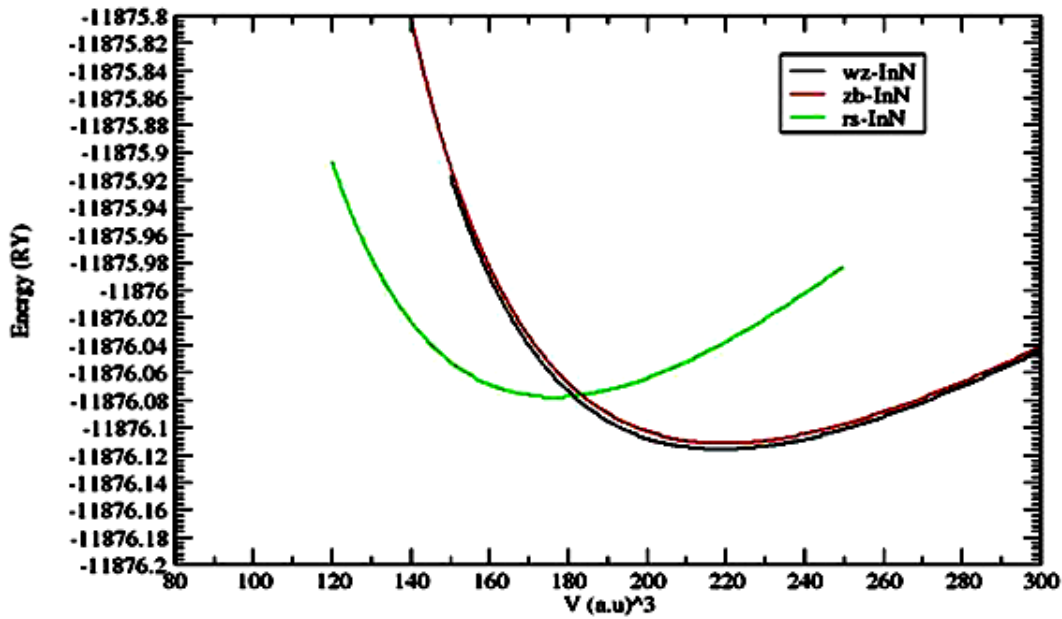


**Figure (4.28): The transition pressure of InN using GGA method**

In table 4.14 the transition pressure  $p_t$  from WZ to RS is found to be 16.6 GPa and from ZB to RS is 18.5 GPa. These results are close to experimental values. The ground state of InN is the WZ structure.

## Chapter 5

### Conclusion

The full-potential linearized augmented plane wave (FP-LAPW) approach within the density functional theory (DFT) in the local density approximation (LDA) and the generalized gradient approximation (GGA) for the exchange correlations functional is used to calculate bulk properties, ground-state energies, lattice parameters, bulk modulus, its derivatives, equation of state, transition pressure, energy band gap and band structures.

Using FP-LAPW method we have obtained the following results:

- 1- The calculated structural parameters ( $a$ ,  $B$ ,  $B'$ ) using FP-LAPW method are found to be in good agreement with the available experimental data and other theoretical results.
- 2- The phase transition for AlN compound occur from WZ to RS and from ZB to RS. The transition pressure from WZ to RS is found to be 9.3 GPa, 10 GPa and the transition pressure from ZB to RS is found to be 3 GPa, 4.64 GPa for LDA and GGA calculations respectively.
- 3- For InN compound, the phase transition from WZ to RS and from ZB to RS is found to be at 16.6 GPa, 18.5 GPa for GGA calculations, respectively.
- 4- For BN compound, the phase transition from ZB to RS is found to be at 500 GPa for GGA calculation.

- 5- The energy band gaps for AlN compound are calculated for WZ, RS and ZB structures is found to be 4.425 eV, 4.032 eV, 2.70 eV and 4.179 eV, 4.341 eV, 3.275 eV for LDA and GGA calculations, respectively.
- 6- For InN compound, the energy band gap is calculated for WZ, RS and ZB structures which is found to be -0.264 eV, 0.083 eV, -0.3896 eV and -0.3643 eV, -0.277eV, -0.51361eV using LDA, GGA and calculations, respectively.
- 7- For BN compound the energy band gap is calculated for RS and ZB structures, which is found to be 2.193, 1.710 eV and 4.356, 4.433 eV using LDA, GGA and calculations, respectively.
- 8- This study shows that AlN compound is insulator for WZ, ZB and RS structures in both GGA and LDA calculations, while the BN compound is semiconductor for RS and ZB in LDA calculations, and insulator for RS and ZB in GGA calculations. In addition, the InN compound is semimetal for WZ, RS and ZB in both GGA and LDA calculations.
- 9- AlN and InN compounds can be found in WZ structures as a ground state and originally in WZ structure since this structure has a minimum binding energy.
- 10- BN compound can be found in ZB structures as a ground state and originally in ZB structure since this structure has a minimum binding energy.

## REFERENCES

- [1] K. Mohammed Benali, **First-Principle Study of Structural, Elastic and Electronic properties of AlN and GaN Semiconductors under Pressure Effect and Magnetism in AlN :Mn and GaN:Mn systems.** Doctor's Thesis. Abou-Bakr Belkaid University-Tlemcen, 2 (2004).
- [2] S. Berrah, H. Abid, A. Boukortt, M. Sehil, **Turk.J.Phys.** **30**, 513 – 518 (2006).
- [3] J. L. F. Da Silva, C. Stampfl, J. Neugebauer, and M.Scheffler, **Physical Review.** **B65**, 245212 (2002).
- [4] S. Nakamura, M. Senoh, S. Nagahma, N. Iwasa, T. Yamada, T. Matsuahita, H. Kiyoku, and Y. Sugimoto Jpn, **J. Applied Phyics.** **35/** (1996), p.174.
- [5] Z.H. Levine and St.G. Louie. **Physical Review.** **B 25**, 6310 (1982).
- [6] D. Fritsch, H. Schmidt, and M. Grundmann, **Physical Review.** **E 67**, 235205, (2003).
- [7] N. E. Christensen, I. Gorczyca, **Physical Review.** **B 50**, 4397 (1994).
- [8] [http:// www.ioffe.rssi.ru/SVA/NSM Semicond/InN/basic.htm](http://www.ioffe.rssi.ru/SVA/NSM_Semicond/InN/basic.htm).
- [9] D.Bagayoko, L.Franklin, and G.L. Zhao, **J.Applied Physics.** **96**,4297 (2004).

- [10] A. G. Bhuiyan, A. Hashimoto, and A. Yamamoto, **J.Applied Physics**. **94**, 2779 (2003).
- [11] T. L. Tansley and C. P. Foley, **J.Applied Physics**. **59**, 3241 (1986).
- [12] J. Wu, W. Walukiewicz, K. M. Yu, J. W. Ager III, E. E. Haller, H.Lu, W. J. Schaff, Y. Saito, and Y. Nanishi, **J.Applied Physics**. Lett. **80**, 3967 (2002).
- [13] T. Matsuoka, H. Okamoto, M. Nakao, H. Harima, and E. Kurimoto, **J.Applied Physics**. Lett. **81**, 1246 (2002).
- [14] A. P. Lima, A. Tabata, J. R. Leite, S. Kaiser, D. Schikora, B. Sch ttker, T. Frey, D. J. As, and K. Lischka, **J. Cryst. Growth**.201/202, 396 (1999).
- [15] V. Cimalla, J. Pezoldt, G. Ecke, R. Kosiba, O. Ambacher, L.Spie , H. Lu, W. J. Schaff, and G. Teichert,. **J.Applied Physics**. Lett. **83**, 3468 (2003).
- [16] N. E. Christensen and I. Gorczyca, **Physical Review**. B **50**, 4397 (1994).
- [17] L. Bellaiche, K. Kunc, and J. M. Besson, **Physical Review**. B **54**, 8945 (1996).
- [18] [http://en.wikipedia.org/wiki/Aluminium\\_nitride](http://en.wikipedia.org/wiki/Aluminium_nitride).
- [19] W. Yong-Liang, C. Hong-Ling, Y. Bai-Ru, and C. Xiang-Rong, **Theor. Phys**. **49**, 489–492 (2008).

- [20] M. Suzuki, T. Uenoyama, and A. Yanase, **Physical Review. B** **52**, 8132 (1995).
- [21] J. Li, K. B. Nam, M. L. Nakarmi, J. Y. Lin, and H. X. Jianga, **J.Applied Physics. Lett.** **83**, 25 (2003).
- [22] J. H. Edgar, S. Strite, I. Akasaki, H. Amano, C. Wetzel, *Properties, Processing and Applications of Gallium Nitride and Related Semiconductors*. 264 (1999).
- [23] J. Li, K. B. Nam, M. L. Nakarmi, J. Y. Lin, and H. X. Jiang, Manhattan, P. Carrier, S. WeiAppl, **J.Applied Physics. Lett** **83**, 5163 (2003).
- [24] I. Petrov, E. Mojab, R.C. Greene, L.Hultman and J. E. Sundgren, **J.Applied Physics. Letter.** **60**, 2491(1992).
- [25] M. J. Paisley and R. F. Davis, **J. Cryst. Growth.** 127 136 (1993).
- [26] J.H. Edgar, *Properties of group III nitrides* .Institution of Electrical Engineers, London, 1994.
- [27] Y. N Xu and W. Y Ching, **Physical Review. B** **48**, 4335(1993).
- [28] F. Litimein1, B. Bouhafs, and P. Ruterana, **New Journal of Physics** **.4**, 64.1–64.12 (2002).
- [29] [http://en.wikipedia.org/wiki/Boron\\_nitride](http://en.wikipedia.org/wiki/Boron_nitride).
- [30] [http://en.wikipedia.org/.../Ab\\_initio\\_quantum\\_chemistry\\_methods](http://en.wikipedia.org/.../Ab_initio_quantum_chemistry_methods).

- [31] R. M. Wentzcovitch, S. Fahy, M. L. Cohen, and S. G. Louie, **Physical Review B** **38**, 6191 (1988).
- [32] K. Albe, **Physical Review B** **55**, 6203 (1997).
- [33] <http://en.wikipedia.org/wiki/DFT>.
- [34] P. Hessler, N. T. Maitra, K. Burke, **Journal of Chemical Physics** **117**, 72-81 (2002).
- [35] E. Runge, E. K. U. Gross, **Physical Review Letters** **52**, 997 (1984).
- [36] O. J. Wacker, R. Kummel, E. K. U. Gross, **Physical Review Letters** **73**, 2915 (1994).
- [37] <http://www.physics.ohio-state.edu/~aulbur/dft.html>.
- [38] P. Hohenberg, W. Kohn, **Physical Review** **136**, 864–871 (1964).
- [39] G. Vignale, Rasolt, Mark, **Physical Review Letters** **59**, 2360–2363 (1987).
- [40] <http://chemistry.ncssm.edu/book/Chap9DFT>.
- [41] W. Kohn and L. J. Sham, **Physical Review** **140**, A1133 (1965).
- [42] R. G. Parr and W. Yang, **Density-Functional Theory of Atoms and Molecules. Oxford Science Publications**, 145-147 (1989).
- [43] Richard M. Martin, **Electronic Structure Basic Theory and Practical Methods**. Cambridge University Press, 173 (2004).

- [44] [http:// en.wikipedia.org/wiki/Density\\_functional\\_theory](http://en.wikipedia.org/wiki/Density_functional_theory).
- [45] J. Dobson *et al*, **Physical. Review. Lett** **96**, 073201(2006).
- [46] J. Tao and John P. Perdew, **Physical. Review. Lett.** **95**, 196403 (2005).
- [47] J. P. Perdew and A. Zunger, **Physical. Review. B** **23**, 5048 (1981).
- [48] D. M. Ceperley and B. J. Alder, **Physical. Review. Lett.** **45**, 566 (1980).
- [49] [http:// cmt.dur.ac.uk/sjc/thesis/thesis/node13.html](http://cmt.dur.ac.uk/sjc/thesis/thesis/node13.html)
- [50] R. O. Jones and O. Gunnarsson, **Rev. Mod. Phys.** **61**, 689 (1989).
- [51] S. H. Vosko, L. Wilk, and M. Nusair, **Can. J. Phys.** **58**, 1200 (1980).
- [52] K. Burke, J. P. Perdew, and M. Levy, in *Modern Density Functional Theory*, J. M. Seminario and P. Politzer, Eds . Elsevier, Amsterdam (1995).
- [53] A. D. Becke, **Physical. Review. A** **38**, 3098 (1988).
- [54] P. Bagno, O. Jepsen and O. Gunnarsson, **Physical. Review. B** **40**, 1997 (1989).
- [55] A. D. Becke, **J. Chem. Phys.** **97**, 9173 (1992).
- [56] D. Porezag and M. R. Pederson, **J. Chem. Phys.** **102**, 9345 (1995).
- [57] D. R. Hamann, **Physical. Review. Lett.** **76**, 660 (1996).

- [58] G. Ortiz, **Physical Review B** **45**, 11 328 (1992).
- [59] M. Petersen, F. Wagner, L. Hufnagel, M. Schffler, P. Blaha, and K. Schwarz. **Computer Physics communications** . **126**, 294-309 (2000).
- [60] D. J. Singh, **Physical Review B**. **60**, 16359–16363 (1999).
- [61] P. Blaha, K. Schwarz, P. Sorantin, S.B. Trickey, **Comput. Phys. Commun.** **59**, 399 (1990).
- [62] P. Blaha, K. Schwarz, P. Herzig, **Physical Review Lett.** **54**, 1192 (1985).
- [63] B. Winkler, P. Blaha, K. Schwarz, **Am. Mineralogist** **81**, 545 (1996).
- [64] B. Kohler, P. Ruggerone, S. Wilke, M. Scheffler, **Physical Review Lett.** **74**, 1387 (1995).
- [65] X. G.Wang, W. Weiss, Sh.K. Shaikhutdinov, M. Ritter, M. Petersen, F. Wagner, R. Schlgl, M. Scheffler, **Physical Review Lett.** **81**, 1038 (1998).
- [66] M. Bockstedte, A. Kley, J. Neugebauer, M. Scheffler, **Comp. Phys. Commun.** **107**, 187 (1997) .
- [68] K .Schwarz, P.Blaha and Madsen, G. K. H, **Comp.Phys.Commun** (2001).

- [69] Weinert M., Wimmer E., and Freeman A. J, **Physical. Review. B** **26**, 4571 (1982).
- [70] Yu R., Singh D. and Krakauer H., **Physical. Review. B** **43**, 6411(1991).
- [71] Bl chl P.E., Jepsen O. and Andersen O.K., **Physical. Review. B** **49**, 16223 (1994).
- [72] [http:// www.siliconfareast.com/physics/zinc-blende.htm](http://www.siliconfareast.com/physics/zinc-blende.htm)
- [73] P. Blaha, K. Schwarz, G.K.H. Madsen, D. Kvasnicka, J. Luitz, WIEN2k, *An augmented plane wave plus local orbitals program for calculating crystal properties*. Vienne University of Technology, Vienna, Austria, (2001).
- [74] F. D. Murnaghan, **Proc. Natl Acad. Sci. USA**, **30**, 244 (1944).
- [75] H. J. Monkhorst and J.D. Pack , **Physical .Review. B** **13**, 5188 (1976).
- [76] J. Furthmüller, P. H. Hahn, F. Fuchs, and F. Bechstedt, **Physical. Review. B** **72**, 205106 (2005).
- [77] K. Kim, W. R. L. Lambrecht, and B. Segall, **Physical .Review. B** **50**, 1502 (1994).
- [78] M. Van Schilfgaarde, A. Sher and A. B. Chen, **J. Cryst. Growth.** **178**, 8 (1997).

- [79] A. Trampert, O. Brandt and K. H. ploog, in Crystal Structure of Group III Nitrides, edited by J. I. Pankove and T.D. Moustakas, **Semiconductors and Semimetals.50** (1998).
- [80] A.F. Wright, J. S. Nelson, **Physical Review. B** **51** 7866 (1995).
- [81] C.Y. Yeh, Z.W. Lu, S. Froyen, and A. Zunger, **Physical .Review. B** **46**, 10086 (1992).
- [82] C. Stampfl and C.G. Van de Walle, **Physical .Review . B** **59**, 5521 (1999).
- [83] J. Serrano, A Rubio, E. Hernandez, A. Munoz and A. Mujica, **Physical .Review. B** **62**, 16612 (2000).
- [84] Q. Xia, H. Xia, and A. L Ruoff, **J. Applied Physics** **.73**, 8198 (1993).
- [85] H. Vollstadt, E. Ito, M. Akaishi, S. Akimoto, and O. Fukunaga, **Proc. Jpn. Acad.** **66**, 7 (1990).
- [86][http://www.chem.ufl.edu/~reynolds/member\\_resources/images/BarryThompson\(2005\).](http://www.chem.ufl.edu/~reynolds/member_resources/images/BarryThompson(2005).)
- [87] Hilmi, Unlu, **Solid State Electronics.** **35**, 1343-1352 (1992).
- [88] <http://ece-www.colorado.edu/~bart/book/eband5.htm>.
- [89] L.I. Berger, **Semiconductors Materials.** 124 (1997).
- [90] [http:// encyclopedia.kids.net.au/page/gi/Gibbs\\_free\\_energy](http://encyclopedia.kids.net.au/page/gi/Gibbs_free_energy).

- [91] A. Tadjer, B. Abbar, M. Rezki, Mzt. **Chem. Phys.** **62**, 75 (2000).
- [92] Knittle, R. M. Wentzcovitch, R. Jeanloz and M. L. Cohen. **Nature**, 337-349 (1989).
- [93] A. Zaoui, F. EL Haj Hassan, **Journal of Physics**. 253-262 (2001).
- [94] S. Saib, N. Bouarissa. **Physica B** **387**, 377-382 (2007).
- [95] K. Kim, W. R. L. Lambrecht, and B. Segall, **Physical Review B** **53**, 16310 (1996).
- [96] B. Daoudi, M. Sehil, A. Boukraa, H. Abid. **Int. J. Nanoelectronics and Materials**. **1**, 65-79 (2008).
- [97] M. Ueno, M. Yoshida, A. Onodera, O. Shimomura, K. Takemura, **Physical Review B** **49**, 14 (1994).
- [98] Q. Xia, H. Xia, and A. L. Ruoff, **J. Applied Physics**. **B 8**, 345 (1994).
- [99] [www.springerlink.com/index/p475w85547npw808](http://www.springerlink.com/index/p475w85547npw808).

جامعة النجاح الوطنية  
كلية الدراسات العليا

دراسة تغيرات الحالة لكل من المركبات نيتريد الألمنيوم  
ونيتريد البورون ونيتريد الأنديوم تحت ضغط عال باستخدام  
طريقة FP-LAPW

إعداد

حنين يوسف سعيد شلش

إشراف

د.محمد سلامة أبو جعفر

د.عبد الرحمن أبو لبدة

قدمت هذه الأطروحة استكمالاً لمتطلبات الحصول على درجة الماجستير في الفيزياء  
بكلية الدراسات العليا في جامعة النجاح الوطنية بنابلس، فلسطين.

2009م

ب

دراسة تغيرات الحالة لكل من المركبات نيتريد الألمنيوم  
ونيتريد البورون ونيتريد الإنديوم تحت ضغط عال باستخدام

**طريقة FP-LAPW**

إعداد

حنين يوسف سعيد شلش

إشراف

د.محمد سلامة أبو جعفر

د.عبد الرحمن أبو لبدة

**الملخص**

في السنوات السابقة لم يلفت الأنتباه نوع آخر من مواد أشباه الموصلات علميا وتجاريا  
مثما لفتت الأنتباه مجموعة النتريدات الثلاثة (InN و BN و IN)

ويرجع سبب هذا الاهتمام المتزايد إلى الخصائص الفيزيائية غير العادية التي تتميز بها  
هذه المجموعة والتي يمكن استخدامها في العديد من الابتكارات الالكترونية والالكترونيات  
البصرية ومن الأمثلة الظاهرة على ذلك صمامات الليزر ذات الموجه القصيرة والتي تستفيد من  
الفجوة العريضة لأحد مكونات هذه المجموعة وهو AIN.

كما أن مركب InN كان من المتوقع أن يكون مادة مناسبة للابتكارات الالكترونية  
مثل ترانزستورات ذات انتقالية عالية نتيجة لكتلته الفاعلة.

إن اعتماد التآلق الضوئي على الضغط يعتبر مهم جدا في فهم الطاقة الالكترونية  
والخواص التركيبية والمكونات الصلبة في أشباه الموصلات.

إن اثر الضغط على الخواص الالكترونية للمواد (InN و BN و AIN) يمكن  
استقصاؤه باستخدام كلا الطريقتين التجريبية والنظرية.

في هذه الأطروحة تم الاعتماد على أسلوب الجهد المزيد والتام ذو الموجات المستوية  
الخطية والذي يعمل تحت برنامج حاسوب يسمى (WIEN2K) والذي يعتمد على نظرية كثافة

الشحنات داخل الذرات حيث يستخدم فيها أسلوبين للتقريب وهما (LDA) و (GGA) في تحديد مستويات الطاقة المستقرة وخصائص أخرى من تركيب (WZ) و (ZB) و (RS) لكل من المركبات (InN و BN و AIN).

ولقد تم حساب معادلات الحالة (EOS' s) في تركيبات (RS) و (WZ) و (ZB) لمركبات AIN و BN و InN.

أهم النتائج التي تم التوصل إليها:

1. إن الحسابات الحالية تتوافق بشكل جيد جدا مع البيانات التجريبية والحسابات النظرية الأخرى.
2. إن مركب AIN يعتبر بمثابة عازل في جميع تراكيبه.
3. إن مركب BN يعتبر شبه موصل في حسابات LDA وعازل في حساب GGA.
4. إن مركب InN يعتبر شبه معدني في جميع تراكيبه.
5. تم تحديد طاقة الفجوة لمركب AIN لجميع تراكيبه وهي (4.42، 4.032 2.7) إلكترون فولت على طريقة LDA بينما بلغت قيمة طاقة الفجوة (4.17 4.34 3.275) إلكترون فولت على طريقة GGA.
6. بلغت قيمة طاقة الفجوة لمركب BN (2.163، 4.36) إلكترون فولت على طريقة LDA (1.71 4.43) إلكترون فولت على طريقة GGA.
7. بلغت قيمة طاقة الفجوة لمركب InN (0.264- 0.0838 0.3896) إلكترون فولت على طريقة LDA بينما بلغت قيمة طاقة الفجوة (0.3643- 0.277- 0.5136) إلكترون فولت على طريقة GGA.

8. أما فيما يتعلق بمركب AIN فانه تم تحديد الإنتقال التركيبي وحساب الضغط الانتقالي من تركيب WZ إلى RS الذي بلغ 10 جيجا باسكال ومن ZB إلى RS 4.64 جيجا باسكال باستخدام طريقة GGA بينما كان مقدار الضغط الإنتقالي من تركيب WZ إلى RS يساوي 9.3 جيجا باسكال ومن تركيب ZB إلى RS 3 جيجا باسكال باستخدام طريقة LDA.

9. بينما بلغ مقدار الضغط الإنتقالي لمركب InN من تركيب WZ إلى RS 6.6 جيجا باسكال ومن تركيب ZB إلى RS 18.5 جيجا باسكال.

10. بلغ مقدار الضغط الإنتقالي لمركب BN من تركيب ZB إلى RS 500 جيجا باسكال.

This document was created with Win2PDF available at <http://www.win2pdf.com>.  
The unregistered version of Win2PDF is for evaluation or non-commercial use only.  
This page will not be added after purchasing Win2PDF.